Electrochemistry of Titanium Carbide MXenes in Supercapacitor

Tingting Jiang,* Yichen Wang, and George Z. Chen*

Novel electrode materials are always explored to achieve better performance of supercapacitors. Titanium carbide MXenes, $Ti_3C_2T_x$, are one of the very promising candidates for electrode materials in supercapacitors due to their unique structural and ion storage properties as 2D materials. Their large specific surface area, adjustable functionalized surface terminals, high electrical conductivities, hydrophilicity, and high Faradaic capacitance, also known widely but confusingly as pseudocapacitance, are highly desirable for making high-performance electrodes with increased dis-/charging rates and capacities. Herein, some selective electrochemical considerations of $Ti_3C_2T_x$ MXenes for uses in supercapacitors are critically reviewed and assessed, aiming at a better fundamental understanding of the electrochemical basics and processes in $Ti_3C_2T_x$ MXene-based electrode materials for supercapacitor applications.

1. Introduction

With the depletion of fossil energy resources and the deterioration of the environment, the goals to reaching the carbon emission peak and carbon neutrality have been proposed and agreed around the world. Green and sustainable energy sources including wind tide and sunlight have gained much attention with the relevant technologies grown for years to replace the fossil-based traditional ones. However, intermittency and the strong dependence on the environment limit the massive and effective application of these renewable energies. A multi-vector and cooperative energy storage infrastructure should be utilized in a post

T. Jiang, Y. Wang
The State Key Laboratory of Refractories and Metallurgy
College of Materials and Metallurgy
Wuhan University of Science and Technology
Wuhan 430081, P. R. China
E-mail: ttjiang@wust.edu.cn
G. Z. Chen
Department of Chemical and Environmental Engineering
Faculty of Engineering
University of Nottingham
Nottingham NG2 7RD, UK
E-mail: george.chen@nottingham.ac.uk

fossil and new energy power station.[1–3] On the other hand, the rapid development of electric vehicles and portable devices has raised new and higher requirements for various energy storage technologies of which electrochemical energy storage (EES) devices are apparently more promising than the others. EES is usually achieved via either or both of two basic charge storage mechanisms: capacitive and Nernstian (or noncapacitive). While Nernstian storage dominates in rechargeable batteries, capacitive storage is the fundamental basis for various supercapacitors. In terms of performance, supercapacitors can provide much larger energy capacity than traditional capacitors and greater power capability than all known rechargeable batteries such as Li-ion batteries.[4–6]

Generally, supercapacitors can be divided into two types according to the energy storage mechanism, namely, electrochemical (or electrical) double-layer capacitors (EDLCs) and pseudocapacitors. In EDLCs, similar to the traditional parallel-plate electrolytic capacitor, an electrical double layer (EDL) forms at the interface of each electrode and the contacting electrolyte where the ions are adsorbed and desorbed reversibly upon potential changes, enabling fast charging and discharging. The difference between EDLC and electrolytic capacitor is simply that the former uses electrodes with much larger specific surface area and hence offers much greater specific capacitance than the latter. In pseudocapacitors, also known as redox supercapacitors, the charges are stored through a redox reaction or Faradaic process at the surface of or in the electrode materials with reversible ingression of ions into the materials to maintain electrical neutrality. The ingression and egression of ions are known as intercalation and deintercalation for materials with appropriate layered or channeled structures. Since charges are stored at the atomic or molecular level via redox reactions, pseudocapacitors usually have higher capacitance than EDLCs. On the other hand, EDLCs show better reversibility, cycle stability, and charge storage rate than pseudocapacitors. Later developments are toward hybrid devices, including asymmetrical supercapacitors that combine the merits of EDLCs and pseudocapacitors, and supercapattery in which both the capacitive and Nernstian storage mechanisms are utilized aiming at improved electrochemical performance.[7]

Electrode materials are essential for all EES devices. Particularly in supercapacitors, carbon materials, including graphene, carbon nanotubes, activated carbons, and carbon aerogels, have

been the most used electrode materials for EDLCs due to their large specific area and excellent electrical properties.[8–12] Transition metal oxides, dichalcogenides, nitrides, sulfides, hydroxides including layered double hydroxides and electronically conducting polymers are typical materials for pseudocapacitors. Meanwhile, there are a large number of emerging electrode materials which store charge following more than one energy storage mechanism.[7,13–15] Nevertheless, pseudocapacitive materials do show some shortcomings such as limited electrical conductivity and unsatisfactory reaction reversibility which are mainly caused by structural instability and poor carrier transportation in the materials. Therefore, the search continues for novel electrode materials that are capable of better performance with particularly increased conductivity and capacity.

As a new family of 2D materials, MXenes have attracted increasing attention since the first successful synthesis in 2011.[16] They are usually transition metal carbides, nitrides, and carbonitrides derived from dozens of MAX phase materials which are unique in their combined metallic and ceramic properties (M: transition metal element, e.g., Ti, Cr, V, or Nb; A: A group element, e.g., Al, Si or Zn, X: C or N). The MAX to MXene conversion involves the removal of the A element and addition of the terminal groups. The general formula of MXene is $M_{n+1}X_nT_x$ (n = 1, 2, 3, or 4), where T_x stands for the surface (or edge) terminal groups including -O, -OH, or -F according to the various synthetic processes and post-treatments.[17–19] More complex compositions and structures, such as bi-metallic MXenes, are also emerging recently.[19] Interestingly, to the authors' best knowledge, the value of x in T_x is not defined in the literature. However, it can be concluded from available literature information that x is nonstoichiometric. Its value should be comparable to that of n for a single-layer structure, but fractional for a few-layer structure, i.e., $x < 1$, because the number of the surface terminal atoms or groups is much smaller than the number of M or X atoms in the structure.

Generally, the synthesis of MXene nanosheets can be achieved via either the top-down or bottom-up methods.[16,20–26] In the former, MXenes are usually etched from the respective MAX phase materials using hydrofluoric acid, fluoride salt, and alkali. Alternatively, electrochemical or molten salt etching, and intercalation are also effective synthesis processes for MXenes. In the bottom-up route, epitaxial growth and sputtering are commonly used.

Similar to another famous 2D material, graphenes, MXenes exhibit unique structural, magnetic, optical, electronic, and electrochemical properties.[27,28] MXenes have been shown to possess great potentials for applications in, e.g., alkali and alkaline earth metal ion batteries and supercapacitors,[16,29–36] electromagnetic shielding,[37] photocatalysis,[38] and water splitting.[39] Due to their remarkable electronic conductivity, good structural stability and flexibility, and tailorable surface functionality, MXenes have been studied as both active electrode materials and current collectors for supercapacitors.[40] The moderate mechanical and easy thin-film forming characteristics also allow MXenes to be used in flexible and wearable devices. Till now, a series of MXenes such as $Ti_3C_2T_x$, Ti_2CT_x, V_2CT_x, and $Nb_2C_3T_x$ have been synthesized and utilized in EES devices, particularly supercapacitors.[41–44] Among the large MXene family, $Ti_3C_2T_x$ is the most investigated and utilized member due to several reasons, such as the readily available MAX phase precursors, conve-

nience in preparation, higher structural stability, and better electronic conductivity. In the following discussion, $Ti_3C_2T_x$ MXenes will be the main focus as a representative of the whole family unless otherwise specified.

It is generally recognized that $Ti_3C_2T_x$ MXenes are capable of exhibiting near-ideal capacitive properties, represented by their highly rectangular cyclic voltammograms (CVs) and almost symmetrical triangular galvanostatic charging and discharging curves (GCDs). These experimental observations were taken by many as evidence of EDL capacitance. This attribution seems to be reasonable because $Ti_3C_2T_x$ MXenes are highly conducting to electrons, and accommodate ions, particularly small metal cations, in their layered structure. However, the multivalence Ti element should enable a certain level of redox activity and hence pseudocapacitance, which was supported by findings from in situ spectroscopic analysis.[45]

On the practical prospect, restacking and aggregation of the MXene sheets during the charge storage process, as well as the unstable surface terminals may deteriorate the electrochemical performance of MXenes in supercapacitors. Several strategies have been developed to solve these problems, such as constructing 3D structures,[46,47] forming heterojunctions with oxides,[48,49] carbons,[50–52] or polymers,[53–56] and modifying the MXene by doping or surface alteration.[57–61] Although there are already several published review articles on the development, synthesis, and properties of MXene-based materials for EES devices,[16–19] there are still some unclear issues on using them for supercapacitors, especially the charge (or energy) storage mechanisms which vary, e.g., in different electrolytes. The device design, including counter electrode and cell configuration may also affect the electrochemical information obtained.

Here, we review and discuss the electrochemistry, or more precisely the features of different electrochemical measurements of $Ti_3C_2T_x$ MXenes for supercapacitor applications, broadly in line with the scheme in **Figure 1**. First, the electrochemical reaction information of MXene as electrode materials in supercapacitors are collated, including CVs and GCDs. Then, the charge (or energy) storage mechanism and the influence of surface terminal groups on the performance are analyzed and summarized. Specifically on pseudocapacitance analysis, the commonly observed Mount Thor-shaped GCDs (see bottom-left of Figure 1 and Section 2.2) are highlighted in association with polarizations that are largely resulting from electrode or cell resistance. For CVs, the confusion on the surface-confined and diffusion-controlled processes in $Ti_3C_2T_x$ MXene electrodes during the charge storage process is clarified. Third, the influence of electrolytes on the electrochemical process of MXenes is outlined. Meanwhile, the advantages and disadvantages of different types of electrolytes for MXene-based supercapacitors are compared, and the related charge storage mechanisms are discussed. It is hoped that this review will provide an improved fundamental understanding of the electrochemical processes of MXene-based electrode materials for supercapacitor applications.

2. Electrochemical Performances of MXene

Due to their application potential in supercapacitors, MXenes including $Ti_3C_2T_x$ have been investigated and reported to offer excellent performance, up to the claimed landmark volumetric
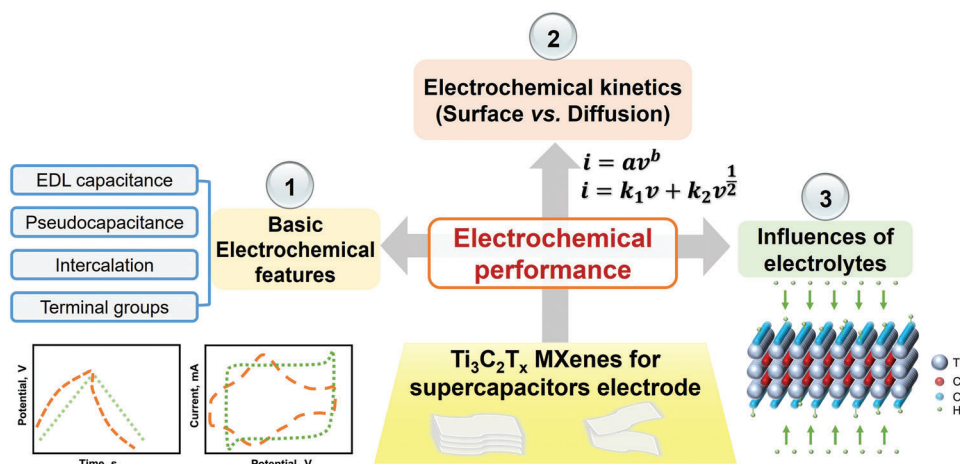
Figure 1. Scheme of electrochemical study of $Ti_3C_2T_x$ MXenes for supercapacitors.

capacitance of 1500 F cm^{-3}, although the reported specific capacitance was only 380 F g^{-1}.[62] In another study, the specific capacitance of $Ti_3C_2T_x$ MXenes was reported as 506 F g^{-1}.[63] Assuming proportional conversion, it should correspond to a volumetric capacitance close to 2000 F cm^{-3},[63] but the reported value was 759 F cm^{-3}.[63] These two examples suggest that the actual density of a MXene material and its packing density on electrode are crucial factors affecting charge storage performance. Therefore further and better understanding of the charge storage mechanism is greatly needed so that the performance of $Ti_3C_2T_x$ MXene electrodes can be improved with high consistency and reliability.

Generally, $Ti_3C_2T_x$ MXenes can exhibit rich capacitive properties which are influenced by the way of atomic connections in each layer or sheet, the surface terminal groups (atoms), the electrode structure and fabrication, and the selected electrolytes. It was reported that according to the relative size of electrolyte cations, the $Ti_3C_2T_x$ MXene could develop a performance that is of either EDL capacitive or pseudocapacitive dominance. When the electrolyte cations were small enough to intercalate between the $Ti_3C_2T_x$ layers with the occurrence of charge transfer, a larger capacitance could result from the redox reactions.[64] On the other hand, larger ions could only form an electrostatic region and therefore the EDLC capacitance was assumed.[65] As for the $Ti_3C_2T_x$ MXene electrode itself, the electrochemical behavior is strongly dependent on the category and amount of the surface terminal groups. Meanwhile, the structure and fabrication of electrodes can also influence the charge storage performance of $Ti_3C_2T_x$ due to the modification of surface area and active sites. In this article, the capacitive properties of $Ti_3C_2T_x$ are summarized in Section 2 (this section). Section 3 will focus on analysis of CVs in terms of surface and diffusion controls, while the effect of electrolytes will be discussed in Section 4.

2.1. Electric Double-Layer Capacitance

Both external and internal surface processes on an electrode (electronic conductor) are important factors affecting the overall capacitance of the electrode. In EDLCs, adsorption and desorption of cations and anions on the electrode surface, including

those internal ones, dominate the energy storage process. Along this line, MXenes, due to their high electronic conductivity and fairly large specific surface area, are expected to benefit from the same charge storage mechanism as that in EDLCs. This seems to be supported by the very rectangular CVs of MXenes as shown in **Figure 2**, corresponding to reported specific capacitance of 150–500 F g^{-1}.[62–64] Considering the fact that the areal capacitance of an EDL is smaller than 40 μF cm^{-2}, the specific surface area of MXenes must be larger than 375 m^2 g^{-1} to enable the value of 150 F g^{-1} in specific capacitance. Unfortunately, in many studies, it was found that MXenes possessed moderate specific surface areas smaller than 100 m^2 g^{-1},[64,65] which is too small to account for the measured specific capacitance. An argument was that in the layered structure of MXenes, intercalated ions were surrounded by water molecules and then combined with metal ions to form an EDL structure on the surface of MXene layer.[66–70]

It can be expected that when the sizes of electrolyte ions and interlayer spacing in MXenes are comparable within a specific range, EDL capacitance should be optimized. Because $Ti_{n+1}X_nT_x$ MXenes are mostly hydrophilic, they should work well in aqueous electrolytes. The fact that they can be terminated by acidic or alkaline groups means that they each would have a preferred acidic, neutral, or alkaline electrolyte. Examples of aqueous electrolytes studied for use with $Ti_{n+1}X_nT_x$ MXenes include H_2SO_4, KOH, $MgSO_4$, and $(NH_4)_2SO_4$.[71,72] Further discussion will be given later on the EDL capacitance of MXenes.

It is worth noting that in most, if not all, reported studies, the capacitive properties of $Ti_3C_2T_x$ MXenes were analyzed using the symmetrical cell configuration as schematically illustrated in Figure 2a. The symmetrical cell is simple to make in laboratory and easy to use for analysis of the cell performance as exemplified in Figure 2b,c in terms of specific or areal capacitance and dis-/charging kinetics. However, the CVs in Figure 2d,e demonstrate that the capacitive potential range (CPR) of MXenes are usually negative and narrower than 1.0 V in aqueous electrolytes. These facts make it more desirable to couple the MXene electrode with a positive electrode (positrode) of a different material, e.g., hydrous manganese oxides, $MnO_x \cdot \alpha H_2O$ or polypyrrole,[3] whose working potential range is more positive to form an
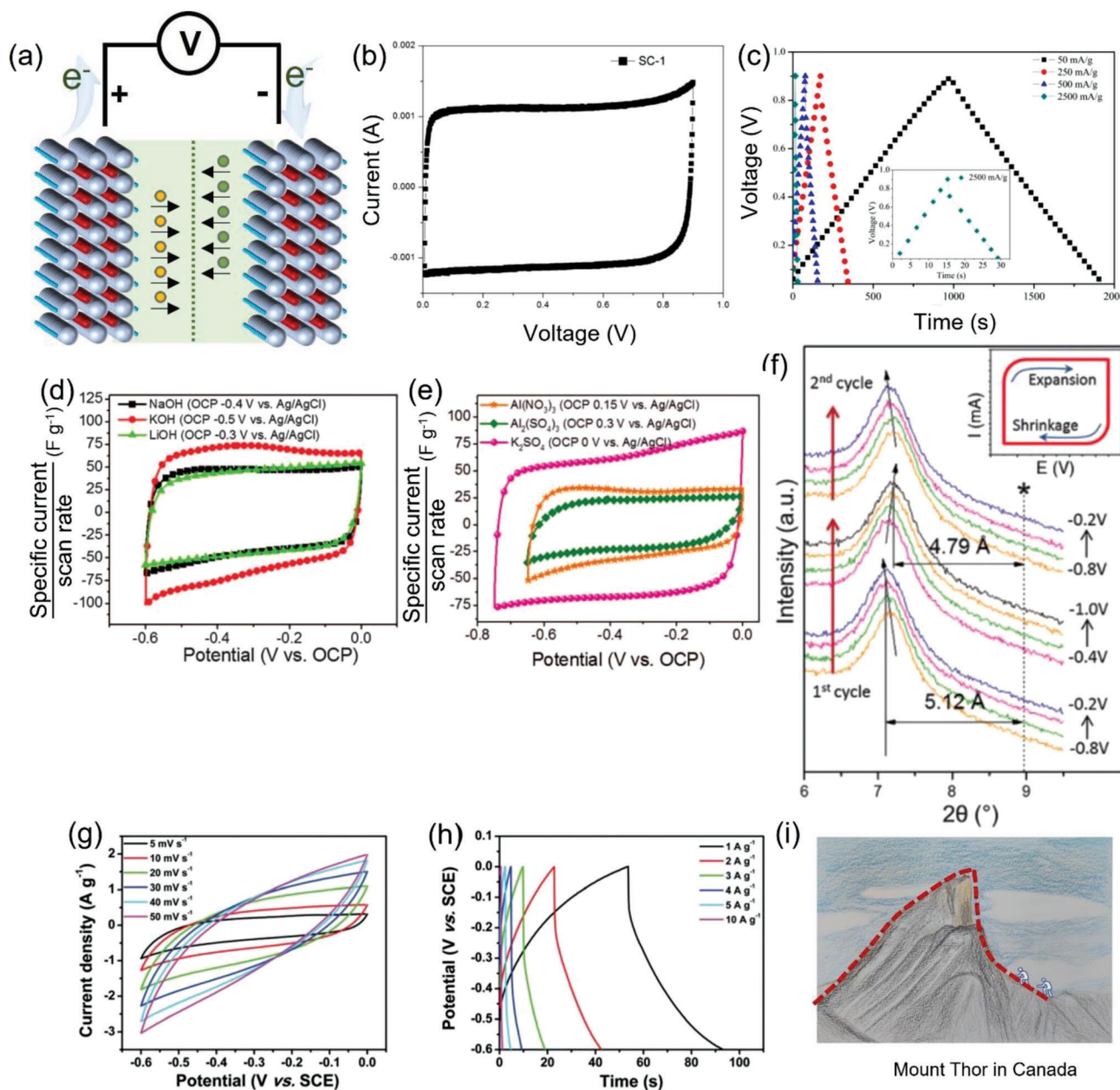
Figure 2. a) Schematic illustration of a symmetrical EDLC. b) A CV at 1 mV s^{-1} and c) GCD curves at different currents of symmetrical Ti$_3$C$_2$T$_x$ MXene supercapacitors with an aqueous electrolyte of 3 M KOH. Reproduced with permission.[66] Copyright 2015, Springer Nature. d,e) CVs at 20 mV s^{-1} of Ti$_3$C$_2$T$_x$-based electrodes in various aqueous electrolytes. f) Electrochemical in situ X-ray diffraction (XRD) patterns of multilayer exfoliated Ti$_3$C$_2$T$_x$ MXene in 1 M KOH solution. Reproduced with permission.[71] Copyright 2013, American Association for the Advancement of Science. g) Fish-shaped CVs and h) Mount-Thor-shaped GCD curves of a very resistive Ti$_3$C$_2$T$_x$ MXene electrode in simulated seawater. Reproduced with permission.[67] Copyright 2018, the Royal Society of Chemistry. i) Authors' impression of Mount Thor in Canada[73] whose peak outline resembles very much the shape of the black GCD curve in (h).

asymmetrical supercapacitor. Further, it is also possible to build a supercapattery which combines a supercapacitor (or capacitive) electrode with a battery (or Nernstian) electrode.[3] It should be pointed out that Ti$_{n+1}$X$_n$T$_x$ MXenes are among the very few known pseudocapacitive materials that can work in a negative potential window, making them a desirable candidate material of negative electrode (negatrode) for designing new and high-performance EES devices.

Figure 2b shows typical CVs of symmetrical cells of MXenes (with 5 wt% of polytetrafluoroethylene) at a scan rate of 1 mV s^{-1}. The MXenes were prepared by etching Ti$_3$AlC$_2$ with 49% hydrofluoric acid (HF) at 60 °C.[66] The CV exhibited a highly rectangular shape and good symmetry, with a cell voltage up to about 0.8 V, which is similar to that of typical aqueous electrochemical capacitors. According to the GCD curves at various specific currents in Figure 2c, good charge storage reversibility can be

ADVANCED
SCIENCE NEWS

www.advancedsciencenews.com

small
methods

www.small-methods.com

described since the curves are almost ideal isosceles triangles. The capacitance of this $Ti_3C_2T_x$ MXene was found to be about 50 F g^{-1} at a specific current of 1.0 A g^{-1}. This value is significantly smaller than those mentioned above, implying a dominance of the EDL capacitance in the measurement.

The capacitive behavior of $Ti_3C_2T_x$ MXene has been studied under different experimental conditions for practical purposes. For example, Xia et al. built and tested a symmetrical supercapacitor of $Ti_3C_2T_x$ MXene in a seawater electrolyte. Unfortunately, as shown in Figure 2g–i, they recorded sloped fish-like CVs and Mount Thor-shaped GCDs[73] which were obviously distorted from the reversible capacitive performance as shown in Figure 2b–e. They attributed the distortions quite ambiguously to some redox reactive intermediates and products within the mesopores of the electrode.[67] The sluggish features of the distorted CVs and GCDs can indeed be attributed to the effect from electrode or cell polarizations, but high electrode (or cell) resistance is an important experimental factor that has been ignored by many authors in their calculation of capacitance and energy capacity values. A worse scenario is that the ratio of the charge, $Q = It$, and the potential or voltage range, U, measured from the Mount Thor-shaped GCDs were used to calculate the electrode or cell capacitance, $C = Q/U$, or the cell energy capacity, W, according to Equation (1)

$$W = \frac{CU^2}{2} \tag{1}$$

This equation has been derived for both CV and GCD measurements of a supercapacitor cell. Note that C should be the cell capacitance and can be derived from the electrode capacitance according to $\frac{1}{C} = \frac{1}{C_+} + \frac{1}{C_-}$. For a symmetrical cell, $C_+ = C_- = 2C$, where C_+ and C_- are the capacitance of the positrode and negatrode, respectively. Equation (1) can also use mass normalized cell capacitance or specific cell capacitance, C_s, to calculate the specific energy of the cell W_s. For a symmetrical cell, $C_{s+} = C_{s-} = 4C_s$ because the active material mass of the cell is the sum of those of the individual electrodes. For an asymmetrical cell, there is not a simple link between C_s and the specific capacitance of the positrode or negatrode. Instead, the specific cell capacitance needs to be calculated from $\frac{1}{C} = \frac{1}{C_+} + \frac{1}{C_-}$, and $C_s = C/m$, where $m = m_+ + m_-$ is the sum of the active materials masses of both the positrode, m_+, and negatrode, m_-.

To use Equation (1), C must be constant versus the cell voltage, which can only be so when the capacitance of each of the positrode and negatrodes is also constant and independent of the electrode potential. Such requirements are equivalent to using only rectangular CVs or linear and triangular GCDs. The problems from using nonrectangular or peak-shaped CVs or nonlinear or Mount Thor-shaped GCDs for capacitance and energy calculation according to Equation (1) will be discussed later.

Improvement of the overall conductivity and reversibility of the MXene-based electrode can be achieved, e.g., through appropriate combination with activated carbon or carbon black. Such composite electrodes were shown to perform much better due to the synergetic effect of carbon and MXene,[66,68,74–77] although this approach inevitably sacrifices some storage capacity as the specific capacitance of carbon is only a fraction of that of MXenes.

As the performance of EDLCs is strongly dependent on the specific surface area of the electrode materials, high surface areas and porous structures are beneficial to increasing the capacitance of MXene (and also other capacitive materials). However, Lukatskaya et al.[71] prepared a flexible, binder and additive-free $Ti_3C_2T_x$ paper as a supercapacitor electrode in KOH electrolyte, and obtained a volumetric capacitance of 340 F cm^{-3}, much higher than that of a typical EDLC mechanism material (e.g., activated graphene) with the reported surface area. Therefore, the traditional non-Faradaic electrostatic adsorption process may not be the only mechanism for charge storage in MXenes. They further investigated the capacitive behavior of $Ti_3C_2T_x$ MXene in different electrolytes (in Figure 2d,e) and proposed that the cation intercalation should be responsible for the improved capacitance. The CV recorded in K_2SO_4 was mostly rectangular and exhibited higher capacitance than that in electrolytes ($Al_2(SO_4)_3$) of lower electric conductivity. According to their in situ XRD analysis (Figure 2f) during the electrochemical cycling, the c-lattice parameter increased indicated by the downshift of (002) peak. In a later study, the same group used electrochemical in situ X-ray absorption near edge structure spectroscopy (XANES) to detect the valence change of the Ti element.[61] Their findings further supported the dominant redox contribution to the measured capacitance in line with the pseudocapacitive attribution.

Although there are increasing experimental findings supporting the pseudocapacitive nature of $Ti_3C_2T_x$ MXene, the EDL storage mechanism can still not be excluded. Instead, the proportion of EDL capacitance, although relatively small, varies according to the properties, conductivity in particular, and macro- and microstructures of the $Ti_3C_2T_x$ MXene electrodes, and also the nature of electrolyte, conditions of measurements and setup of the electrode or supercapacitor cell.

2.2. Pseudocapacitance

An important feature of charge storage in MXenes is ion intercalation between the layers of MXenes, which is expected to be selective by the ion size relative to that of the interspace between the neighboring layers of $Ti_3C_2T_x$ MXenes. The latter also varies between $Ti_3C_2T_x$ MXenes prepared by different fabrication methods. Many authors have used the term "intercalation pseudocapacitance" to describe their experimental observations, but not all ion intercalation processes may lead to the pseudocapacitance for supercapacitors. The truth is that ion intercalation can proceed in either capacitive or Nernstian materials as will be explained below.

Being layer structured compounds containing the multi-valent Ti element and highly conducting to electrons, $Ti_3C_2T_x$ MXenes are expected to offer redox activities for charge (energy) storage. However, they may present ideal or near ideal capacitive behavior similar to the CVs and GCDs in Figure 2, but also peak-shaped CVs,[45,86] e.g., as displayed in **Figure 3** in line with typical Nernstian (or battery-like) features. Unfortunately, such peak-shaped CVs were claimed to be pseudocapacitive and used for capacitance calculations.

It is worth noting that the overall charge, Q, stored in a cell can be derived from the integration of the current, i, on the CV

**ADVANCED
SCIENCE NEWS**

www.advancedsciencenews.com

**small
methods**

www.small-methods.com
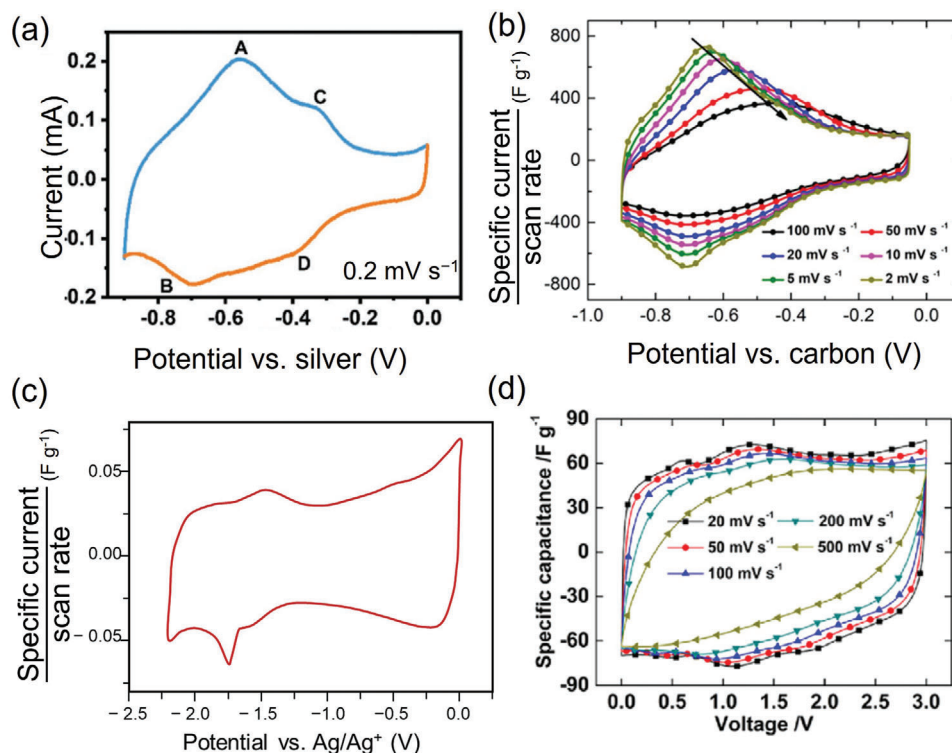
Figure 3. CVs of $Ti_3C_2T_x$ in a) 1 M and b) 3 M H_2SO_4 at indicated potential scan rates. a) Reproduced with permission.[45] Copyright 2019, Wiley-VCH. b) Reproduced with permission.[72] Copyright 2018, Elsevier B.V. CVs of MXene electrode c) at 1 mV s^{-1} in acetonitrile with 1 M $TEABF_4$ and d) in a two-electrode Swagelok cell at scan rate from 20 to 500 mV s^{-1} in a neat ionic liquid of EMI-TFSI. c) Reproduced with permission.[79] Copyright 2022, Elsevier B.V. d) Reproduced with permission.[80] Copyright 2016, Elsevier B.V.

at a scan rate of v ($= U/t$)

$$Q = \int_0^t i \mathrm{d}t = \frac{1}{v} \int_0^{U_{max}} i \mathrm{d}U \tag{2}$$

A similar equation can be written for the overall charge stored in an electrode, replacing U by the electrode potential, E, varying in the given potential range. It is not uncommon in the literature that Equation (2) was applied to nonrectangular CVs, particularly those peak-shaped ones. According to a recent analysis, the "charge/potential range" ratio, i.e., Q/U, from a nonrectangular CV is "nonlinear pseudocapacitance" versus the charge stored in electrode or cell. Such nonlinear pseudocapacitance cannot be used in Equation (1) which is only for the calculation of energy stored in a true supercapacitor whose "linear pseudocapacitance" can be derived from a rectangular CV.[78]

Although materials of nonlinear capacitance should not be used for making a supercapacitor, they can still be used in batteries or supercapatteries. In such cases, the energy capacity can be calculated by integration of the nonlinear GCD curve, or the nonrectangular CV according to Equations (3) and (4), respectively

$$W = i \int_0^{U_{max}} U(t) \mathrm{d}t \quad \text{(for GCDs)} \tag{3}$$

$$W = v \int_0^{U_{max}} i(t) t \mathrm{d}t \quad \text{(for CVs)} \tag{4}$$

where t is the time which can be read directly on GCD, or derived from $U = vt$ on CV with v being the potential scan rate. The current, i, is constant for GCD, but a function of cell voltage for CV.[78] Note that unlike Equation (2) which can be applied to both the cell and electrode, Equations (3) and (4) can only be used for a cell because a single electrode cannot store energy.

It has been shown that Equation (1) is a special case of Equation (3) for GCD when $U(t)$ is a linear function of time which is the feature of capacitive charging and discharging. When $i(t)$ is a constant as that on the rectangular CV of a true supercapacitor, Equation (4) can also be simplified into Equation (1). Therefore, if Equation (1) is used in place of Equation (3) or (4) for nonlinear GCDs or nonrectangular CVs, the calculation would either over- or underestimate the true energy capacity of the cell.

The concept of intercalation pseudocapacitance is worth further consideration. Ion intercalation occurs in response to a difference in chemical or electrochemical potential or both between the electrode and the contacting electrolyte. In all cases, electric neutrality must be maintained in the electrode (and electrolyte), while transport of ions through the electrode material(s) may become a rate control step, invoking kinetic complications. The difference between chemical and electrochemical intercalations is that the former does not involve net charge movement in either the electrode or electrolyte, making no contribution to charge

ADVANCED
SCIENCE NEWS
www.advancedsciencenews.com

small
methods
www.small-methods.com
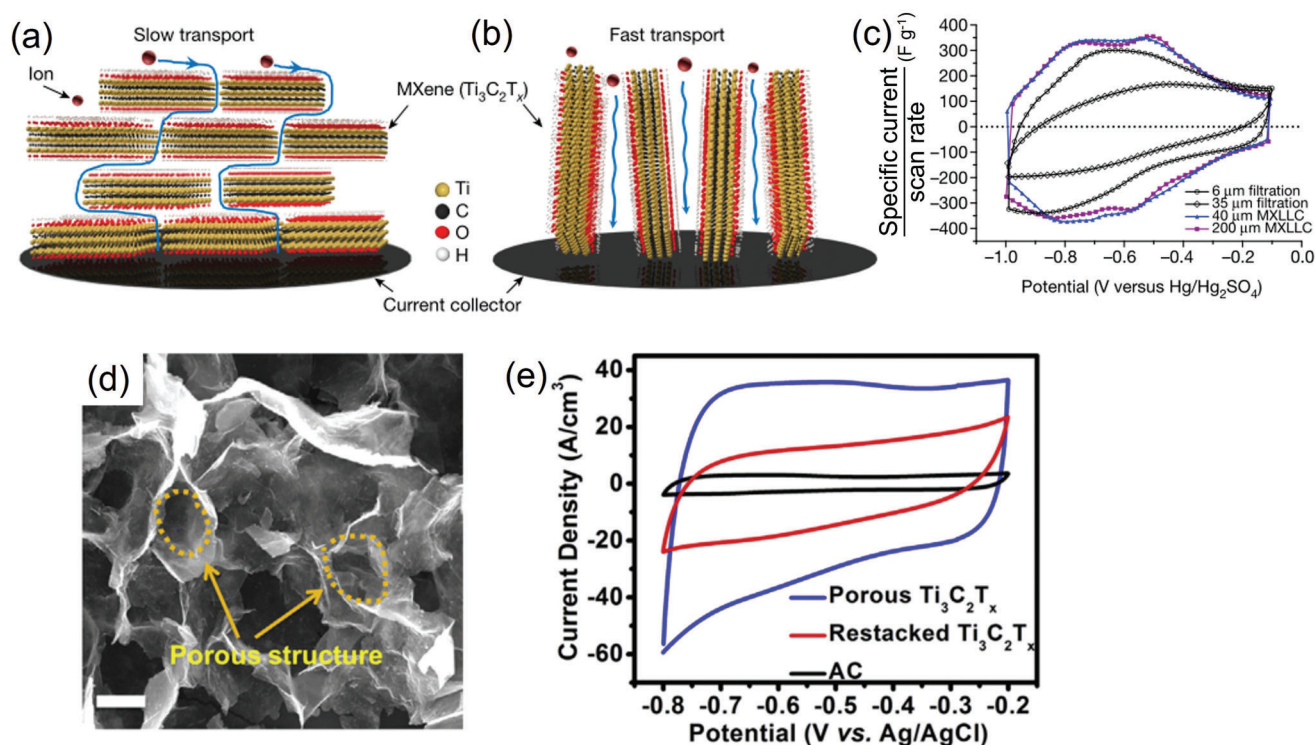
Figure 4. Schematic illustrations of a) restacked and b) vertically aligned $Ti_3C_2T_x$ sheets on electrode surface. c) CVs of $Ti_3C_2T_x$ with different structures and thicknesses at 100 mV s^{-1} in 3 M H_2SO_4. Reproduced with permission.[81] Copyright 2018, Springer Nature. d) FESEM of porous $Ti_3C_2T_x$. e) CVs of porous $Ti_3C_2T_x$, restacked $Ti_3C_2T_x$, and activated carbon at 100 mV s^{-1} in 1 M NaCl. Reproduced with permission.[82] Copyright 2018, Cell Press.

storage. In other words, chemical intercalation may occur spontaneously by simply immersing the electrode in an appropriate electrolyte. Thus, electrochemical intercalation is the only mechanism responsible for charge storage. It may occur according to three different sub-mechanisms, namely, 1) EDL dis-/charging or Faradaic reactions which can be 2) Nernstian or 3) pseudocapacitive. According to a recent analysis,[3] Nernstian storage takes place via the transfer of localized valence electrons at a fixed energy level and hence the peak-shaped CVs, while pseudocapacitance or more correctly Faradaic capacitance reflects the transfer of delocalized valence electrons in a continuous energy band (as that in a semiconductor), leading to rectangular CVs.

The peak-shaped CVs of $Ti_3C_2T_x$ MXenes as shown in Figure 3 reflect well the presence of Nernstian intercalation which is more common in electrode materials of lithium-ion batteries. Comparing the CVs in Figures 2d,e and 3, it is reasonable to conclude that the potential range for recording the CVs plays an important role. In addition, the effect of electrolyte is of great significance as Figures 2d,e and 3 indicate that high proton activity in electrolyte favors the current peak appearing on the CV. In other words, $Ti_3C_2T_x$ MXenes can accommodate both pseudocapacitive (narrow potential range, low acidity) and Nernstian (wider potential range, high acidity) intercalations. In addition, EDL capacitance and hence EDL intercalation are also inevitable in $Ti_3C_2T_x$ MXenes due to their high electronic conductivity and porous structure.

On the electrochemical charge storage mechanism of MXene in supercapacitor electrodes, the structure, particularly designed

structure of MXene may also influence the ion intercalation process which can be reflected on the respective CVs. Restacking and aggregation are the most focused problems for MXene electrode, which may reduce the overall number of active surface sites.

Several novel structures including vertical,[81] pillared,[83,84] 3D porous,[82,85] and crumpled structures[86,87] have been proposed and studied to improve the performance of MXene on electrode via different preparation methods such as freeze-drying, and template assisted. Xia et al.[81] succeeded in coating the electrode surface with vertically aligned $Ti_3C_2T_x$ MXene sheets by mechanical shearing of the discotic lamellar liquid-crystal phase. **Figure 4**a,b schematically shows the structure design and carrier or ion transport pathways in parallelly stacked and vertically aligned MXene sheets on the electrode surface. CVs of the parallel stack of MXene sheets (prepared by filtration) and vertically aligned ones with different thicknesses are compared in Figure 4c, showing strong dependence on electrode structure. The filtered MXene showed the redox peaks at −0.6 and −0.8 V on the CV which disappeared in the thicker film of 35 μm. For the vertically structured MXene film, the pair of redox peaks appeared at −0.4 and −0.6 V, showing no dependence on the film thickness, indicating more effective carrier or ion transport pathways.

As another example proving the effect of electrode structure, Figure 4d shows the scanning electron microscop (SEM) image of a highly crumpled 3D porous matrix of cryo-dried MXene nanosheets after removal of the pore formers and spacers.[82] In Figure 4e, the CV of this porous $Ti_3C_2T_x$ is compared with those of the restacked $Ti_3C_2T_x$ and activated carbon in 1 M NaCl

**ADVANCED
SCIENCE NEWS**

www.advancedsciencenews.com

**small
methods**

www.small-methods.com

solution. It can be seen that this highly porous MXene delivered much larger currents than the restacked one. These examples demonstrate that structurally opening the MXene electrode could provide more surface active sites and promote intercalation of ions which are both beneficial to improving the performance.

2.3. Experimental Findings

Based on the synthesis process, there are abundant surface terminal groups such as -F, -O, -OH on the surface of $Ti_3C_2T_x$ MXenes. In acidic aqueous electrolytes like H_2SO_4, the intercalated proton H^+ is small and easy to transfer between the MXene nanosheets with high ionic conductivity. Then, the protons can bond with the oxygen terminal group on the surface of $Ti_3C_2T_x$ MXene to form a hydroxyl group (**Figure 5**a). The bonding/debonding process between protons and the oxygen terminals on the surface of MXene during the discharging and charging process provide much higher pseudocapacitance than that of EDL capacitance. At the same time, this reversible redox reaction may lead to the transformation in the Ti oxidation valence state from +3 to +4 according to the charging and discharging process, respectively. The corresponding electrochemical reaction is as follows[45]

$$Ti_3C_2O_x(OH)_\gamma F_{2-x-\gamma} + \delta e^- + \delta H^+ \rightarrow Ti_3C_2O_{x-\delta}(OH)_{\gamma+\delta} F_{2-x-\gamma}$$

(5)
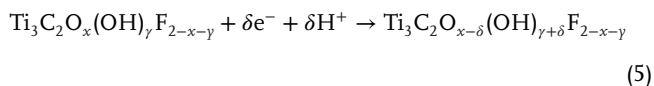
With the smallest ion radius, protons are prone to access the electrochemically active sites on the surface and interface of MXene nanosheets and deliver outstanding cycling and rate performances. In alkaline electrolytes, such as KOH, proton activity is low. The electrochemical behavior of $Ti_3C_2T_x$ MXene as mentioned in Section 2.1, according to available evidence, indicates that the larger metal cation could provide only ion intercalation without interaction with terminal groups.

The electrochemical performance also varies depending on the inherent characteristics of cations. Qian et al.[88] prepared a free-standing film of $Ti_3C_2T_x$ MXene electrode and investigated the behavior during charging and discharging in aqueous electrolytes of LiCl, NaCl, and KCl. An oxidation peak at 0.120 V and a reduction peak at −0.050 V (vs Ag/AgCl) were observed on all CVs in the three electrolytes. The electrochemical performances in KCl and LiCl were better. According to Qian et al., the solvated K^+ ions with fast ion transport could provide a fast electrochemical surface adsorption, resulting in better charge propagation. Small-sized Li^+ ions may be more likely to permeate through the interlayer space between, and adsorb on the MXene nanosheets, delivering good ion storage properties.

In 2014, Ghidiu et al.[25] prepared a paper-like $Ti_3C_2T_x$ clay by etching Ti_3AlC_2 MAX with LiF and HCl, which presented a volumetric capacitance as high as 900 F cm^{-3}, and also showed excellent cyclability. The CVs at different scan rates as shown in Figure 5b demonstrate the good rate capability since the small size of protons could maintain the rapid charge transfer in charging and discharging. The high capacitance and rate capability in 1 M H_2SO_4 agree with the faster and efficient intercalation of the small H^+ ion and its beneficial interaction with the terminal groups.

Cyclic voltammetry can help determine if the intercalation is Nernstian or capacitive or both, but it alone is insufficient to assert between DEL and Faradaic capacitive intercalation. In situ spectroscopy is needed to tell if there is a simultaneous change in the oxidation state of the Ti element in the MXene electrode. Lukatskaya et al.[64] performed in situ XANES for the Ti K-edge to study the changes in the Ti oxidation state during cycling. Shifts in Ti edge energy were monitored, and several spectra were collected according to voltammetric cycling. The potential range was 0.275 to −0.350 V and −0.200 to 0.345 V, respectively. Figure 5c shows the relationship between Ti K-edge energies at half-height of normalized XANES spectra and the applied potentials, where the Ti edge shifted to lower energies in the sweeping from 0.275 to −0.350 V, indicating the decrease in the oxidation state of Ti. The Ti K-edge energies increased to higher levels in the reverse sweeping. By plotting the Ti K-edge XANES spectra at 0.100 and −0.400 V, the average oxidation state can be quantified as shown in Figure 5d, from 2.33 to 2.43 over a 0.7 V wide potential window (Ti oxides are listed as reference).

Mu et al.[45] investigated the charge storage mechanism of $Ti_3C_2T_x$ MXenes in H_2SO_4 by in situ XRD. Figure 5e shows the contour maps of XRD patterns collected with the value of 2θ between 5° and 20° during cyclic voltammetry between 0 to −0.900 V versus Ag, where the obvious shift of the (002) and (006) peaks can be found. The results indicate the change in functional groups instead of the phase transformation during charging and discharging. Correspondingly, the c-lattice parameter changed up to 0.54 Å depending on the potential in the third cycle (Figure 5f). During the charging process, the c value remained above 28.5 Å at first, then decreased quickly from 28.54 to 28.07 Å in the potential range of −0.7 to −0.4 V and gradually expanded to 28.22 Å.

In the discharging process, the c value decreased first to 28.11 Å at −0.600 V and then increased to 28.61 at −0.900 V. The shift of the c-lattice parameter in H_2SO_4 was larger than that in other aqueous electrolytes, and claimed to be in accordance with the higher capacitance of $Ti_3C_2T_x$ MXenes in acidic electrolytes.

Except for experimental results, the Faradaic nature of charge storage in $Ti_3C_2T_x$ MXene in H_2SO_4 electrolyte was also demonstrated by theoretical modeling and calculation based on joint density functional theory with an implicit solvation model and the analysis of Gibbs free energy under a constant electrode potential.[89] It was shown that the surface net charge was mainly distributed on the surface oxygen layer which directly interacted with the electrolyte, as shown in Figure 5g. Based on the proportional relation between the valence and the atomic Bader charge on a Ti atom at different H coverages and electrode potentials, the oxidation state of Ti was found to change from 2.45 to 2.54 at potentials from −0.290 to 0.590 V versus standard hydrogen electrode. This finding is in accordance with the XANES observations.[64] Therefore, the capacitive charge storage of $Ti_3C_2T_x$ MXene in H_2SO_4 is dominated by the redox process or pseudocapacitance. Similar results have been obtained in other types of MXenes, such as V_2CT_x and $Nb_4C_3T_x$.[90]

In organic electrolytes or ionic liquids, similar interactions of ions are thought to have occurred.[80,91–93] According to Figure 3c, the CV of $Ti_3C_2T_x$ MXene at 1 mV s^{-1} in the acetonitrile solution of 1 M $TEABF_4$ (TEA: tetraethyl ammonium) showed predominantly capacitive features. A pair of small and broad peaks at

**ADVANCED
SCIENCE NEWS**

www.advancedsciencenews.com

**small
methods**

www.small-methods.com
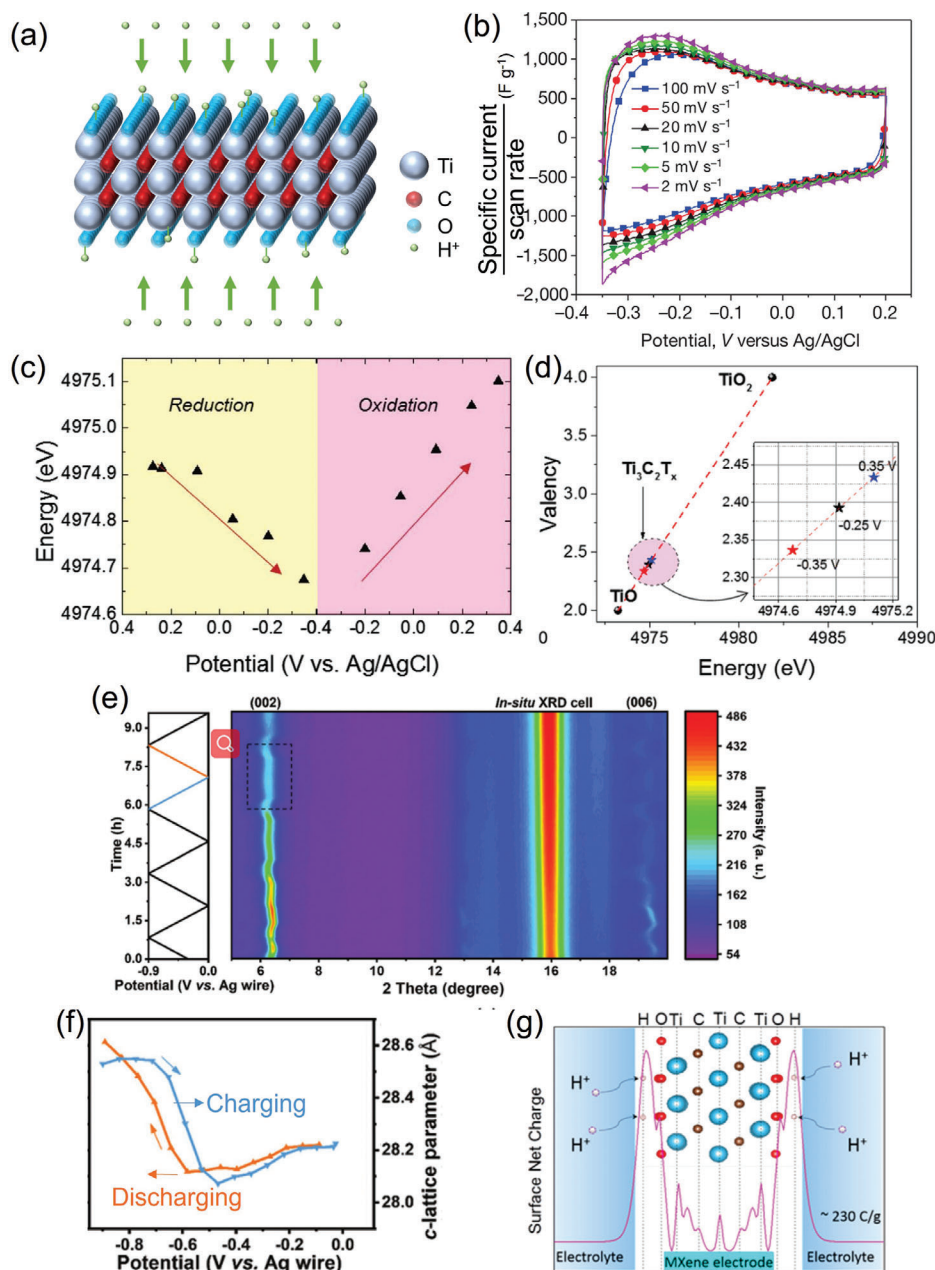
Figure 5. a) Schematic illustration of the redox reaction mechanism. b) CVs at different potential scan rates in 1 M H_2SO_4. Reproduced with permission.[25] Copyright 2014, Springer Nature. c) Variation of Ti edge energy (at half-height of normalized XANES spectra) versus potential between −0.35 and 0.35 V. d) Average Ti oxidation state determination at different applied potentials (see inset). Reproduced with permission.[64] Copyright 2015, Wiley-VCH. e) In situ XRD patterns during electrochemical cycling. f) Change of the c-lattice parameter with potential in the third cycle. Reproduced with permission.[45] Copyright 2019, Wiley-VCH. g) The surface net charge distribution. Reprinted with permission.[89] Copyright 2018, American Chemical Society.

−1.75 and −1.48 V appeared on the CV, and was attributed to the intercalation and deintercalation process of TEA$^+$.[79] Lin et al. also found a couple of peaks at about 0.5 and 1.2 V superposed on the rectangular CV of a two-electrode Swagelok symmetric cell of MXene operating in a neat ionic liquid electrolyte of EMI-TFSI (1-ethyl-3-methylimidazolium bis-(trifluoromethylsulfonyl)-imide) as shown in Figure 3d.[80] These observations in nonaqueous electrolytes are strong indication that Nernstian charge storage

is an intrinsic part of MAXene that can be trigged by not only proton but also other cations.

2.4. Influence of Terminal Groups on the Performance

There are abundant terminal groups on the surface of the as-prepared $Ti_3C_2T_x$ MXene, including -O, -F, and -OH, which are

quite active for further oxidation or contaminations. The reactions of HF with the MAX phase (Ti_3AlC_2) can be listed as follows[43]

$$Ti_3AlC_2 + 3HF = AlF_3 + \frac{3}{2}H_2 + Ti_3C_2 \tag{6}$$

$$Ti_3C_2 + 2H_2O = Ti_3C_2(OH)_2 + H_2 \tag{7}$$

$$Ti_3C_2 + 2HF = Ti_3C_2F_2 + H_2 \tag{8}$$
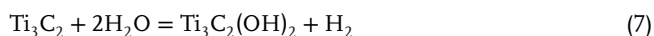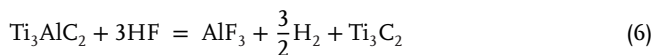
As discussed in the capacitive mechanism of $Ti_3C_2T_x$ MXenes in H_2SO_4 electrolyte, surface terminal groups and surface state play vital roles in the electrochemical behavior of a MXene electrode. Compared to the F-functional groups, the O-functional groups are more favorable since they can form hydrogen bonds with protons in the acidic electrolyte, leading to enhanced capacitance.[94] F-terminal groups occupy the active sites on the surface of MXene but are unknown whether they are involved in any redox charge storage processes, which could hardly provide any capacitive contribution.[95] The intercalation of cation into the interspace between MXene layers could also provide capacitance, and therefore the interlayer space is of great importance. In some cases, the Cl-functional groups on the surfaces could bring about a larger interlayer space in $Ti_3C_2T_x$ MXenes due to the larger atomic size of chlorine and hence could improve the charge transfer during electrochemical cycling.[40]

Therefore, controlling the amount and types of the surface terminal groups of $Ti_3C_2T_x$ MXene with more O-terminals and fewer F-terminals may be an effective way to enhance the capacitive properties of the MXene electrode. Possible approaches to removing -F and -OH and increasing the proportion of -O can be regulation of fabrication method,[95,96] alkaline treatment,[59,95,97] heat treatment,[98] ionic–electronic coupling,[99] and forming composites.[56] It has been reported extensively that $Ti_3C_2T_x$ MXenes with modified surface terminal groups could be obtained by optimizing the preparation methods, the etching agent used, time, and temperatures.[95,96] For example, the general Lewis acidic molten salt etching route for preparing MXenes have been utilized on several types of MAX phase (Ti, Zn, Al, Si, Ga). The molten salts are mostly transition metal halides such as $ZnCl_2$, $CuCl_2$, and $CdBr_2$.[100–105] During the etching process, halide ions such as Cl^- could intercalate into the interlayer space and form the Cl-terminated MXene. Larger interspace sizes caused by Cl-terminals could promote the transfer of protons. However, water dispersible and separated MXenes cannot be obtained through this molten salt route, and KOH treatment is necessary to add -OH terminals on the surface of MXene.[101]

For the as-prepared MXenes, alkaline treatment was found to a facile way to remove -F on the surface due to the unstable Ti–F bond at higher pH.[59] KOH was always used to alkalize $Ti_3C_2T_x$ MXene, where the F-terminals can be replaced by hydroxyl. The following heat treatment can then remove the hydroxyl group and therefore increase the proportion of O-terminals. Li et al.[59] performed surface modification on $Ti_3C_2T_x$ MXenes via KOH solution treatment followed by calcination at 400 °C. The schematic diagram can be seen in **Figure 6**a. After the KOH treatment, XRD analysis revealed an increase in the *c*-lattice parameter with

a larger interlayer spacing. Also, 5% weight loss was detected by in situ thermogravimetric-differential scanning calorimetry-mass spectrometry, corresponding to the removal of terminal-F. Meanwhile, the disappearance of the broadband near 600 cm^{-1} in Fourier transform infrared (FTIR) could be evidence of the removal of -OH after the heat treatment. Figure 6b shows increased capacitance on the CVs of several MXene electrodes after KOH treatment and calcination. All the CVs exhibited similar shapes with a CPR of up to 0.600 V. After K^+ intercalation and the removal of -F and -OH, there was a significant increase of the capacitance (400-KOH-$Ti_3C_2T_x$: 517 F g^{-1} at a discharge current of 1 A g^{-1}). Dall'Agnese et al. and Zhang et al. modified $Ti_3C_2T_x$ MXene by similar means with KOH to achieve higher electrode capacitance.[95,97]

The XRD analysis of heat-treated $Ti_3C_2T_x$ often shows a TiO_2 peak, indicative of partial oxidation.[98] For example, the authors observed the TiO_2 peak on the XRD patterns of $Ti_3C_2T_x$ samples after drying at 80 °C in air. However, in KOH-treated samples without heating, the TiO_2 peak was absent on the XRD pattern.[59] In a detailed electrochemical study of $Ti_3C_2T_x$, it was found that anodic oxidation in 1 M H_2SO_4 at room temperature started at about 0 V versus Hg/HgSO$_4$. XRD analysis also revealed absence of the TiO_2 phase in samples anodically oxidized at different potentials,[106] but there were obvious X-ray photoelectron spectroscopy (XPS) signals of titanium oxyfluoride, $TiO_{2-x}F_x$. Interestingly, the proportion of $TiO_{2-x}F_x$ increased substantially from 8.6% at 0.1 V to 67.4% at 0.9 V, accompanied by a sharp decline of Ti(II) and Ti(III). The obvious increase in F suggests losses of other elements in MXene nanosheets, leaving F to enrich the sample surfaces. As expected, anodic oxidation significantly influenced the electrochemical behavior of MXene in acidic electrolytes. Enhanced storage capacity was recorded at 0.3 V, but the worst scenario occurred at 0.9 V, showing complete loss of redox activity.

Based on the above discussion, it can be concluded that oxidation of MXene can easily occur during the solution, heat, or electrochemical treatment, but the oxidation states or products vary according to the treating process and conditions. Such differences in turn influence the surface chemistry of $Ti_3C_2T_x$ MXene and consequently alter the characteristics of the respective CVs.

Generally, alkaline solutions could hardly eliminate -F thoroughly, so other agents were also selected for surface modification of $Ti_3C_2T_x$ MXene. Based on the transformation of -OH and -X (X, halogen) groups to other groups in nucleophilic reagent, Chen et al.[107] treated MXene with n-Butyllithium (n-BuLi) to improve the electrochemical performance. n-BuLi was used to help replace the -F with -O terminals due to its strong nucleophilicity and reducibility, which can be seen in the schematic diagram in Figure 6c. Figure 6d shows the element distribution in the samples (as-received, LiOH treated, and n-BuLi treated) measured by XPS. After the treatment by LiOH and n-BuLi, the F contents decreased to 8% and 2% from 16% in the as-prepared multilayer and few-layer MXenes. The related capacitance of MXene after n-BuLi modification exhibited great improvement with a capacitance of 523 F g^{-1} at 2 mV s^{-1}.

Annealing is another common way to modify the surface state of MXene. However, oxidation during annealing should be carefully avoided which may deteriorate the energy storage performance.[108] Rakhi et al.[98] investigated the influence of the

**ADVANCED
SCIENCE NEWS**

www.advancedsciencenews.com

**small
methods**

www.small-methods.com

	element				
sample	**Ti**	**O**	**C**	**F**	**N**
HF treated	25.9	30.9	35.7	6.8	0.7
Ar annealed	25.4	31.0	37.6	5.5	0.5
N_2 annealed	26.6	31.1	36.4	4.9	0.9
N_2/H_2 annealed	16.7	22.9	56.8	3.4	0.3
air annealed	21.0	40.9	31.1	6.2	0.8
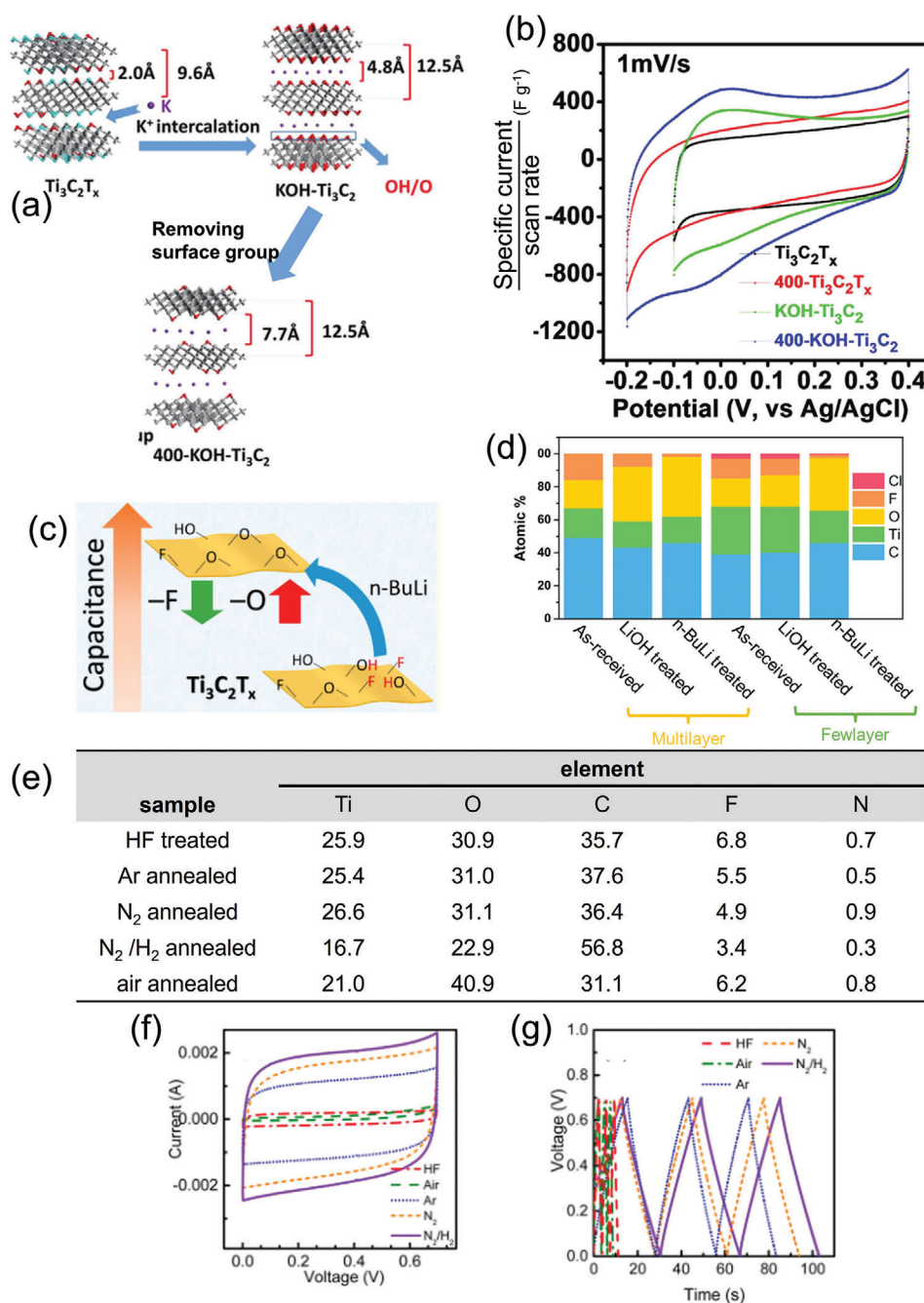
Figure 6. a) Schematic of KOH and post-annealing treatment on MXenes. b) CVs of different samples in 1 M H_2SO_4. Reproduced with permission.[59] Copyright 2017, Wiley-VCH. c) The schematic illustration of the n-BuLi treatment mechanism. d) XPS determined elemental concentrations in samples before and after different treatments. Reproduced with permission.[107] Copyright 2019, American Chemical Society. e) XPS determined elemental concentrations, f) CVs, and g) GCD curves of samples after calcination under different atmosphere. Reproduced with permission.[98] Copyright 2015, American Chemical Society.

annealing atmosphere on the surface structure and then the electrochemical properties of Ti_2CT_x MXenes. After annealing in different atmospheres including Ar, N_2, N_2/H_2, and air, the interlayer space of MXene nanosheets and the surface terminals changed. The atomic concentration of elements in surface layers was collected according to the XPS analysis, as shown in Figure 6e. MXenes annealed under N_2/H_2 had the lowest F con-

centration and highest C concentration. The comparison of CVs of different samples is shown in Figure 6f, revealing a similar electrochemical process but varying specific capacitances by the similar shapes and different areas. Samples annealed in N_2/H_2 presented the largest capacitance. Figure 6g shows the GCDs of these samples with near-ideal triangular shapes. An obvious capacitance improvement was obtained in the three annealed

**ADVANCED
SCIENCE NEWS**

www.advancedsciencenews.com

**small
methods**

www.small-methods.com

samples. Therefore, annealing under a specific atmosphere is an effective way to modify the surface terminals of Ti_2CT_x MXene for enhanced electrochemical performances in supercapacitors.

Electrochemical activation could also regulate the surface state of MXene and therefore improve the electrochemical performance by introducing more and/or deeper reactive sites. Jung et al.[109] conducted electrochemical activation of a composite of $Ti_3C_2T_x$ and graphene by 300 CV cycles between −0.50 and 0.50 V versus Ag/AgCl in the aqueous electrolyte of Na_2SO_4. This activation treatment was thought to have expanded the stacked nanosheets via interactions with Na^+ ions, which in turn brought about more reaction sites for charge storage via more efficient intercalation and deintercalation of cations such as Mg^{2+}. Besides, for the V_2CT_x MXene, performing an initial charging in an aqueous electrolyte of 3 M $ZnSO_4$ and 1 M Li_2SO_4 at 1.4, 1.8, and 2.0 V versus Zn/Zn^{2+} for 2 h could oxidize or regulate the valence of surface V atoms without changing the inner structure of V-C-V, while the resulting VO_x at the surface as well as the original electroconductive inner structure could further ensure the fast and high capacity charge storage.[110]

3. Surface-Confined and Diffusion-Controlled Processes

To gain further insight into the electrochemical process in MXene electrodes, CVs are often recorded at a wide range of scan rates and analyzed for information on the relevant reaction kinetics or charge transport dynamics. The current response, i, of an electrode coated with a layer of charge storage material, either EDL or Faradaic capacitive, or Nernstian, can be expressed as a function of the scan rate, v, by either of the mathematically equivalent Equations (9)–(11)[32,111–113]

$$i = av^b \tag{9}$$

or

$$\log(i) = \log(a) + b\log(v) \tag{10}$$

$$i = k_1 v + k_2 v^{\frac{1}{2}} \tag{11}$$

where a, b, k_1, and k_2 are constants that can be determined experimentally. The value of b is in the range of 0.5–1 for charge storage in an electrode or supercapacitor cell. In the strict sense, the current can include two contributions, the surface-confined and the diffusion-controlled processes. Generally, the linear relationship of i with v ($b = 1$, $k_2 = 0$) means surface control, or $v^{1/2}$ ($b = 0.5$, $k_1 = 0$) implies diffusion control. By determining the coefficients, the contributions from each of the two processes can be distinguished and deconvoluted.[4,78,114,115] The value of b can be determined readily by the slope in the linear fitting of the plot of $\log(i)$ versus $\log(v)$ according to Equation (10).

It is worth noting that the principle behind Equations (9)–(11) has been well known for an electrode process under the surface-diffusion mixed control, but it was first applied in analysis of capacitive charge storage by Liu, Pell, and Conway (LPC) in 1998.[114] This LPC method was later used by Wang, Polleux, Lim, and Dunn (WPLD) in their analysis of the CVs of TiO_2 nanoparticles.[116] They calculated the values of the $k_1 v$ and $k_2 v^{1/2}$ terms in Equation (11) for all potentials of the forward and backward scans of the CV and claimed the obtained "$k_1 v$ versus potential" curve to be the pseudocapacitive contribution or capacitance. They then attributed the $k_2 v^{1/2}$ term as the insertion contribution or intercalation capacity. Till now, many researchers have applied the LPC method in their analyses of CVs of charge storage materials with reference to the work of WPLD, instead of that of LPC. This is likely because of the WPLD claim of the separation of pseudocapacitance from intercalation capacity, which is however incorrect and misleading. Similarly, the LPC method has been applied for the analysis of the CVs of MXenes but there are some different understandings of how to define the charge storage process and mechanism.

As discussed above, the capacitance of $Ti_3C_2T_x$ MXene is influenced by EDL, intercalation of cations, and interactions between the surface terminals of MXene (e.g., -O) and the cations (e.g., H^+) in the electrolyte. The EDL capacitance was generally considered to be a fast surface-confined process. Other than EDLC, there are some disagreements and confusion on how to define the kinetic and/or dynamic processes.

In the first case, the surface-confined contribution ($b = 1$) was defined directly as the capacitive storage, and the other process was defined as the diffusion-limited process ($b = 0.5$).[25,62,107,117] In some reports, the diffusion-controlled part was directly considered as the bulk process (or the battery type).[72] Lukatskaya et al.[62] conducted the electrochemical measurements of three porous MXene electrodes with different loading masses in 3 M H_2SO_4 at scan rates from 20 to 10 000 mV s⁻¹. They then determined the slope b of the log (i) versus log (v) plot (**Figure 7**a,b). For the electrode with the lowest loading mass, b was nearly 1 at scan rates up to 3 V s⁻¹. In the other two electrode films with medium and highest loading masses, b was around 1 only at scan rates lower than 2 and 1 V s⁻¹, respectively, but approached 0.5 at higher scan rates. These observations agree very well with the expected influence of diffusion which would become more difficult and hence control the current flow at higher scan rates and/or through thicker coatings. Wang et al.[117] proposed a similar opinion on diffusion-controlled and surface-confined processes. They derived the value b close to 1 with the same means in lithium bis(trifluoromethanesulfonyl)imide (LiTFSI) with the polycarbonate (PC) solvent. Some other reports revealed the same results, where the contribution of surface-confined process (they defined as the capacitive part) dominated the whole process in the energy storage of MXene-based supercapacitors.

In another opinion, the two current contribution parts were defined as the surface capacitive ($b = 1$), and the diffusion-limited ($b = 0.5$). The former consisted of EDL capacitance and pseudocapacitance, and the latter was believed to be the intercalation pseudocapacitance. The capacitance could therefore be expressed as follows[116,118]

$$C = \frac{i(V)}{v} = k_1 + k_2 v^{-0.5} \tag{12}$$

Li et al.[59] conducted alkaline treatment and annealing on their prepared MXene samples, and then performed electrochemical investigations in 1 M H_2SO_4 at scan rates from 1 to 20 mV

ADVANCED
SCIENCE NEWS

www.advancedsciencenews.com

small
methods

www.small-methods.com
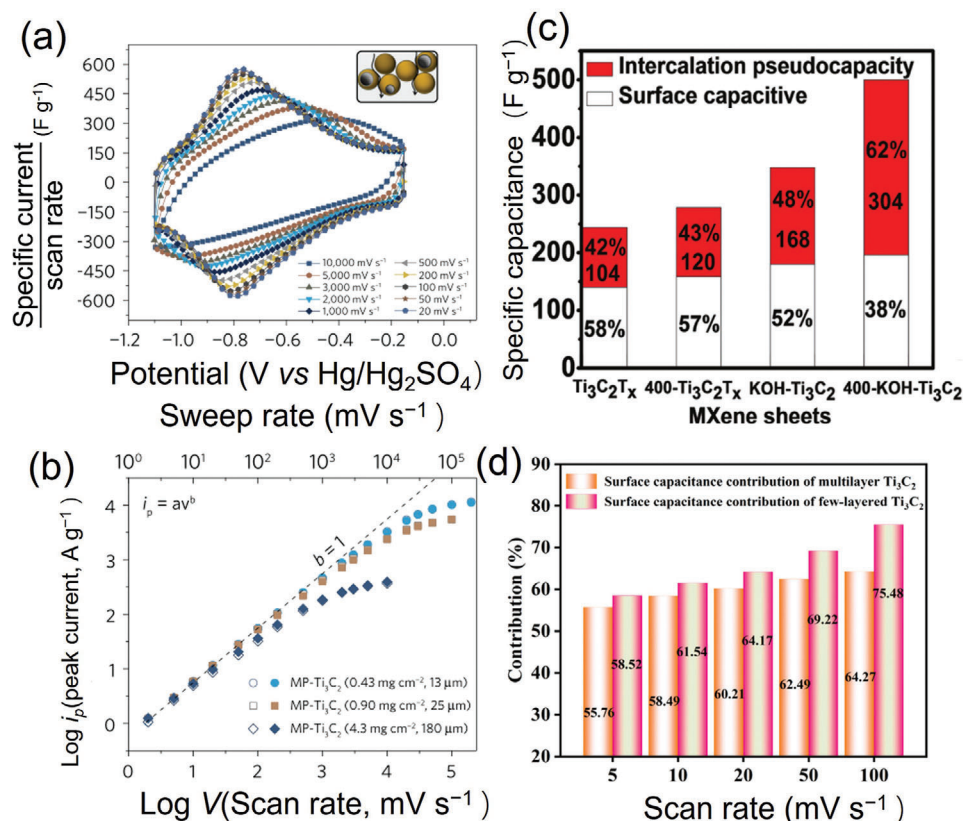
Figure 7. a) CVs of $Ti_3C_2T_x$ MXene at indicated scan rates in 3 M H_2SO_4 with the inset showing the schematic porous structure. b) Determination of the slope, *b*, on the log (*i*) versus log (*v*) plots of electrodes with different mass loading and thickness of $Ti_3C_2T_x$ MXene. Reproduced with permission.[62] Copyright 2017, Springer Nature. c) Comparison of the surface and diffusion (intercalation) contributions to the overall capacitance for different MXene sheets. Reproduced with permission.[59] Copyright 2017, Wiley-VCH. d) Comparison of surface contributions to the overall capacitance at different scan rates for multilayer and few-layer MXenes. Reproduced with permission.[120] Copyright 2021, Springer Nature.

s^{-1}. Figure 7c shows the contribution distributions at 1 mV s^{-1} for $Ti_3C_2T_x$ electrodes undergoing different treatments. At low scan rates, there was an obvious contribution from the diffusion-limited part, which became relatively lower at higher scan rates. For the KOH-treated and annealed electrode, the intercalation pseudocapacitive part contributed 62% to the overall capacitance, much higher than those of other samples. It was believed that after treatment, the intercalation and subsequent redox reactions on the surface of MXene were enhanced due to the larger proportion of active -O terminals in the $Ti_3C_2T_x$ electrodes. The same analysis was conducted on an asymmetric supercapacitor of $RuO_2//Ti_3C_2T_x$.[119] It was found that the diffusion-controlled contribution derived from the Faradaic intercalation process was about 25% at the scan rate of 50 mV s^{-1} in 1 M H_2SO_4.

Some reports evaluate the current contribution simply by the original definition of the fast surface-reaction contribution and the slow diffusion-controlled contribution. Cho et al.[121] performed CV analysis on a binder-free MXene electrode in 1 M H_2SO_4 at different scan rates and obtained a proportion of 93% contributed from the surface reaction part by deconvolution. In the same way, Wu et al.[120] prepared multilayer and few-layer by microwave-assisted method and compared the kinetics of these two electrodes in 3 M KCl at different scan rates. The deconvolution results are shown in Figure 7d. The capacitance of the few-

layer MXene came from the joint contribution of surface capacitance and diffusion-limited process. The surface-confined contribution increased at higher scan rates.

Generally, it is not reasonable enough to simply define the surface-confined part as a capacitive contribution. Diffusion may play an indispensable role in the intercalation of cations into MXene nanosheets. Otherwise, there is a lack of consideration to conclude the diffusion-controlled part as the intercalation pseudocapacitance, where one should think over the surface redox reaction. In fact, for comprehensive and complicated energy storage processes on MXene electrodes in a supercapacitor, the use of "surface-confined" and "diffusion-controlled" is extensively accepted.

It is clear from the above discussion on the few but typical examples of reported studies that confusions and erroneous interpretations are common place on the CVs of $Ti_3C_2T_x$ MXenes (and other materials showing pseudocapacitive or Faradaic capacitive properties). First of all, the specific charge capacity and capacitance, including EDL capacitance and pseudocapacitance, are potential- and time-independent thermodynamic property with a quantitative nature for a given material. However, both surface-confined and diffusion-controlled charge transfer and transport processes are kinetic or dynamic phenomena which are time dependent. The potential and time dependence of these two

processes are well reflected by the fact that the values of the two terms in Equation (11) vary significantly with the potential and potential scan rate, as evidenced in Figure 7d. Second, whether an electrode process is surface-confined or diffusion-controlled or both, i.e., mix controlled depends on the time scale of measurement and/or the conditions of the electrode, particularly the thickness (loading per unit area) and porosity of the active material. Figures 7b and 6c are strong evidence of this understanding. Last, but not the least, both capacitive and noncapacitive (or Nernstian) charge storage can be surface-confined or diffusion-controlled or both. Even charge storage via the EDL capacitive mechanism can be slowed by diffusion, while ion intercalation does not always suffer from the diffusion, particularly at low scan rates and in thin coatings. Therefore, it is meaningless and misleading to attribute the two terms in Equation (11) to either charge capacity or capacitance. There is no doubt that Equations (9)–(11) are useful and helpful for understanding the charge storage mechanisms, dynamics, and kinetics, their significance should not be overestimated. It is worth noting that in practice, diffusion control should be avoided or minimized when designing and fabricating an electrode for all EES devices.

4. Influence of Electrolytes

Despite many advantages, there are still some obstacles in the application of $Ti_3C_2T_x$ MXenes as supercapacitor electrodes. The self-restacking of MXene nanosheets due to the strong Van der Waals interactions may deteriorate the structure stability and charge transfer rate and therefore degrade the electrochemical performances. Besides, the unstable surface terminals, the limited width of the potential window, and the possible oxidations of MXene nanosheets may together impede the further application of MXene as capacitive electrodes. Several strategies and novel designs have been proposed to solve these problems and further promote the electrochemical properties such as energy capacity and power capability of MXene-based supercapacitors. In particular, modification of the electrolyte to match with the MXene electrode and novel electrode structural and composition designs is proven effective approaches.

Electrolytes play multiple and vital roles in the electrochemical mechanism and performance of the supercapacitor. They determine the electrode potential and cell voltage windows, affect both the EDL and Faradaic capacitances (and also the Nernstian capacity), provide the ions for charge transfer and transport processes to maintain electric neutrality, control the rate and reversibility of charge storage, particularly ion intercalation or ingression, and ensure the safety of all EES devices.

In this section, the influence of several types of electrolyte on the electrochemical performance of MXene, including the potential or voltage window, safety, capacitance, and charge transfer rate will be discussed. **Figure 8** shows a comprehensive comparison of the effects of different types of electrolyte on the performances and safety of MXene-based supercapacitors, such as aqueous, organic, ionic liquid, and water-in-salt (WIS) electrolytes.

The charge storage mechanisms of $Ti_3C_2T_x$ MXene in aqueous electrolytes such as H_2SO_4 and KOH have been discussed in Section 2, including EDL capacitance and pseudocapacitance that involves intercalation of ions and interactions between ions
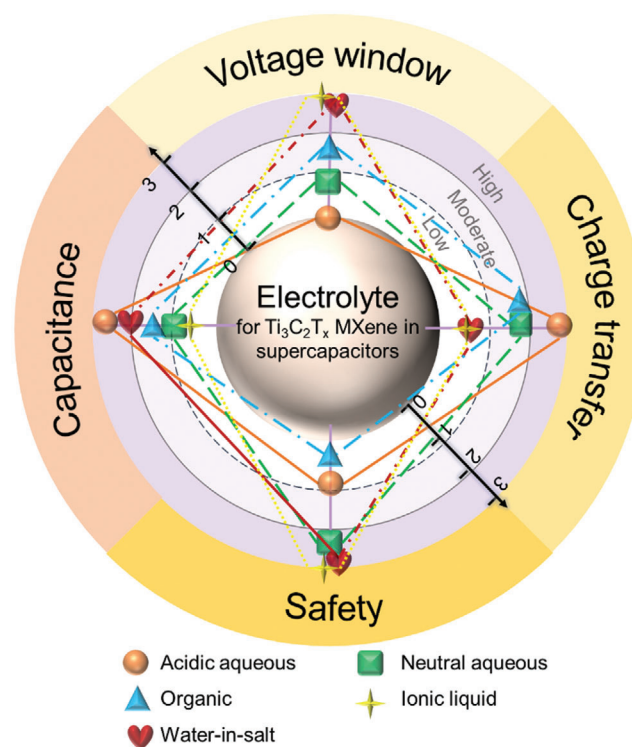
Figure 8. Comparison of different electrolytes for $Ti_3C_2T_x$ MXene-based supercapacitors.

and surface terminals. Due to the surface reactions between O-terminals and protons, $Ti_3C_2T_x$ MXenes exhibit usually higher capacitance in acidic electrolytes. Nevertheless, neutral aqueous electrolytes are more environmentally friendly and can improve the safety of the supercapacitor. Also, most current collectors used (e.g., Cu foil, Al foil, and Ni foam) are unstable in acidic conditions. Besides, in aqueous electrolytes, the hydrogen and oxygen evolution reactions (HER and OER) would theoretically occur at cell voltages higher than 1.23 V (the decomposition voltage of water). In some cases where the electrode materials have high overpotentials for either or both HER and OER, such as carbon and lead, a cell voltage beyond 2.0 V may be achieved. This is well known for the lead-acid battery with a nominal cell voltage of 2.1 V, while some laboratory carbon//carbon and carbon//MnO_x supercapacitor cells also worked up to 2.0 V.[122,123] Nevertheless, the voltage window of aqueous electrolyte is still not large enough for the demand of high voltage of supercapacitors with larger energy capacities.[72,88,124–126]

To expand the electrode potential and cell voltage windows and gain a larger energy capacity, one of the most viable methods is to use electrolytes with higher stability. Organic solvent-based and ionic liquid electrolytes have been proven to enlarge the voltage window of MXene-based supercapacitors to about 2.4[117,127] and 3.0 V,[80,128,129] respectively. In organic electrolytes or ionic liquids, the energy storage process is considered different from that in aqueous electrolytes. Since the surface terminal groups -F and -O terminals on $Ti_3C_2T_x$ MXene are electrochemically inactive in the organic electrolyte, the EDL storage mechanism is dominant in an organic or ionic liquid electrolyte, where ions in

**ADVANCED
SCIENCE NEWS**

www.advancedsciencenews.com

**small
methods**

www.small-methods.com
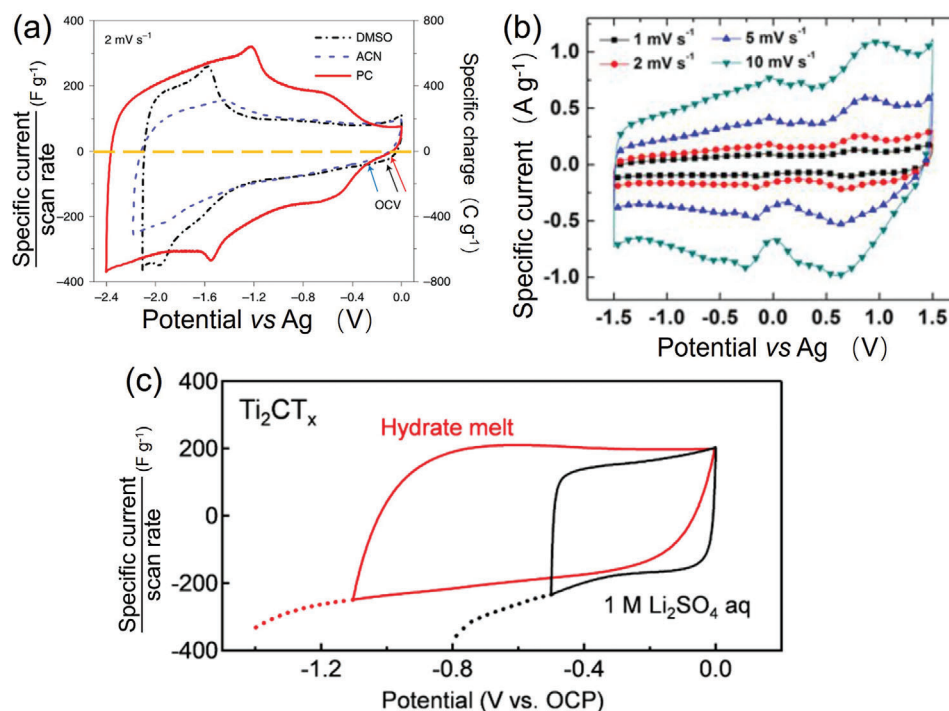
Figure 9. a) CV of $Ti_3C_2T_x$ MXene in three organic electrolytes at a scan rate of 2 mV s^{-1}. Reproduced with permission.[117] Copyright 2019, Springer Nature. b) CV of $Ti_3C_2T_x$ MXene in a neat EMI-TFSI electrolyte at indicated scan rates. Reproduced with permission.[132] Copyright 2016, Elsevier. c) Ti_2CT_x MXene in a neutral aqueous electrolyte of 1.0 M Li_2SO_4 and hydrate melt of Li(TFSI)$_{0.7}$(BETI)$_{0.3}$·2H$_2$O, TFSI: bis-(trifluoromethanesulfonyl)imide, BETI: bis-(pentafluoroethanesulfonyl)imide. Reproduced with permission.[133] Copyright 2019, American Chemical Society.

electrolyte such as EMI$^+$ and TFSI$^-$ may intercalate between the $Ti_3C_2T_x$ MXene nanosheets in the positive and negative potential windows, respectively.[93] **Figure 9**a compares the potential windows for the CVs of $Ti_3C_2T_x$ MXene at a scan rate of 2 mV s^{-1} in the electrolytes of 1 M LiTFSI in dimethyl sulfoxide, acetonitrile (ACN), and PC, which could widen the voltage window to 2.1, 2.2, and 2.4 V, respectively.[117] It can be seen in Figure 9a that the PC-based electrolyte showed the best electrochemical performance with a larger charge capacity and wider potential window. The Coulombic efficiency was found to be 96% with a claimed discharge capacitance of 195 F g^{-1} (468 C g^{-1}).

It is worth noting that the CVs in Figure 9a all show current peaks, but the authors still derived "specific capacitance" by normalizing the current, i, of the CV against the potential scan rate, v, and the mass of active material on the electrode, m, using the equation

$$C = \frac{i}{vm} \tag{13}$$

Obviously, for a nonrectangular CV, C derived from Equation (9) is a variable against the potential and, strictly speaking, is not really the characteristic specific capacitance of an active material. However, many authors have applied Equation (9) in their analyses of CVs for the convenience of comparison between CVs recorded at different scan rates and mass loading on the electrode. The caution is on labeling the vertical axis of the CV with a title of "specific capacitance (F g^{-1})" or similar which can be confusing.

In fact, EDL capacitance in diluted electrolyte varies with electrode potential as has long been described in textbooks of electrochemistry. Such potential-dependent EDL capacitance is termed as "differential capacitance".[130] It is logical to extend this term for EDL capacitance to pseudocapacitance. When normalized against the mass of active material on electrode, the term changes to "specific differential capacitance" with the unit of F g^{-1}. By doing so, the possible confusion with the specific capacitance for an active electrode material can be avoided.

Jackel et al.[131] observed the reversible volume expansion of MXene in ionic liquids due to the ion in electrolytes spontaneously intercalates into the interlayer space of $Ti_3C_2T_x$ nanosheets. This preintercalation, i.e., chemical intercalation, caused swelling of the material and apparently prevented restacking of the MXene sheets which in turn improved electrochemical cycling at the negative potentials. Lin et al.[132] investigated the electrochemical performance of $Ti_3C_2T_x$ MXene in neat EMI-TFSI electrolytes, which provided enhanced properties in a 3 V wide potential range from −1.5 to 1.5 V versus Ag. The CVs at different scan rates can be seen in Figure 9b. Combining with in situ XRD, it was found that the interlayer spacing of MXene nanosheets decreased during positive polarization, which might have resulted from the electrostatic attraction between the intercalated cation and MXene nanosheets, or the deintercalation of cations.

Besides, WIS electrolytes have attracted much attention recently due to their relatively wide potential windows, good stability against hydrogen evolution, and eco-friendliness without organic solvents. Wang et al.[93] proposed a desolvation-free

Li^+ insertion charging mechanism of $Ti_3C_2T_x$ MXenes in WIS electrolytes, which presented a diffusion-controlled process. Reversible expansion and shrinkage were also observed as the solvated Li^+ ions entered and exited the $Ti_3C_2T_x$ MXene electrode. Based on WIS, hydrate melt electrolyte is another selection for improving the energy storage properties of MXene supercapacitor by increasing the potential range. Kim et al.[133] realized the high-density intercalation of hydrated Li^+ in the interlayer of Ti_2CT_x MXene nanosheets with a larger voltage window (Figure 9c).

Compared to aqueous electrolyte, wider potential or voltage windows could be obtained by the organic, ion liquid, and WIS electrolytes, but they also have other drawbacks. For organic electrolytes and ion liquids, poor conductivity due to partly the large ion size may limit the ionic charge transfer and transport in the supercapacitor, leading to decreased charge/discharge rate. Meanwhile, organic electrolytes are always flammable, volatile, toxic, and expensive, which limits their application in supercapacitors from the perspective of safety and economy. The WIS electrolyte exhibits moderate safety and enhanced voltage window, but the capacitance and conductivity of ions are just acceptable. Although with the low-voltage window, the aqueous electrolyte is low-cost and highly conductive, and has high ion concentration. Therefore, for future applications of $Ti_3C_2T_x$ MXene in supercapacitors, the modification and combination of electrolytes should be further investigated and considered.

For information and future references, the performances of supercapacitor electrodes of $Ti_3C_2T_x$ MXenes are summarized in **Table 1**, showing particularly high values in specific and volumetric capacitances. Strong influences are also evidenced from electrolytes, materials morphologies and structures, and hybrid or composite designs of different dimensionalities such as 2D layered, 3D porous, and vertically aligned coatings on electrode.

5. Summary and Perspectives

MXenes, especially $Ti_3C_2T_x$ MXenes exhibit excellent prospects for applications as electrode materials in supercapacitors due to their fairly high electronic conductivities, 2D layered structure, and tailored surface chemical states. MXenes-based electrodes can provide high specific capacitance involving redox chemistry of Ti, and ion intercalation and interaction with surface terminal groups, and good rate performance in supercapacitors. Materials and electrode structure design and compositing with other materials have been proposed to achieve better electrochemical performances. Understandings are clarified on the electrochemical mechanism of MXenes-based electrodes during the charge storage process. According to the selection of electrolyte, charges can be stored by electrostatic adsorption of cations on the surface of MXene, intercalation of cations into the interlayer space between MXene nanosheets, or the surface redox reactions between surface terminals of MXene (e.g., -O) and protons H^+. Analyses of the diffusion-controlled and surface-confined contributions to the current on CVs are also carried out according to the electrochemical basics. Particularly, some literature confusion and errors are clarified and corrected. Furthermore, electrolytes which show significant effects on the electrochemical process of energy storage in MXene-based supercapacitors are also discussed from the aspects of reaction mechanism, electrochemical perfor-

mance, and safety issues. It is hoped that the above discussions may provide some basic and clear information on the related electrochemistry and help further research to achieve better improved performance of $Ti_3C_2T_x$ MXene in supercapacitors.

There are some issues remaining for future research and practical application as listed and discussed below.

1) The synthesis of $Ti_3C_2T_x$ MXene should be optimized to be low-cost, high-yield, and eco-friendly. Both the current preparation process and the MAX phase precursor are expensive. The most-used method is the etching process which involves HF or F-based salt reagents. The safety and security risks and upscaling of production should be considered. The synthetic process will affect the types and proportions of surface terminal groups, the interlayer spacing, and the number of layers, which subsequently influence the final properties. Therefore, precise and controllable synthesis should be considered in future investigations to obtain ideal micro- or nanostructures, adjustable chemical compositions, and active sites.

2) MXenes are prone to oxidation and degradation in water or humid air due to the reaction between H_2O and surface defects which are highly active sites, leading to the loss of intrinsic physical and chemical properties. The synthetic process such as the etching conditions, defect density, size of the MXene nanosheet, and surface terminals may all influence the oxidative degradation of MXene. Therefore, the stability of $Ti_3C_2T_x$ MXene against oxidation should be maintained or improved by using suitable working conditions, e.g., in an inert atmosphere at low temperatures, modified synthetic techniques with less vacancies, and surface modification.

3) More MXenes to enlarge the MXene family will be sought with the aid of both the experimental and modeling methods. A deeper and better understanding is needed on their structures and compositions, and the correlation with electrochemical performances and potential applications.

4) Structural modifications including the 3D structure, porous structure, and compositing with other materials such as carbon, transition metal compounds, and polymers have been proven effective to achieve a more stable electrode with better carrier transportation. The balance between specific and volumetric capacitances should be considered.

5) Aqueous electrolytes can lead to higher capacitance and faster charge transport, but their relatively narrow potential windows are often a concern in various applications. Organic or ionic liquid electrolytes can expand the potential window to a large extent, but the capacitance and rate performance are still unsatisfactory. How to combine the advantages of these two kinds of electrolytes is a direction of future effort.

6) There are still some unclear issues in the mechanisms of the charge or energy storage process, e.g., the intercalation mechanism of different ions into MXene nanosheets with various spacing, the theoretical capacitance of MXenes when cooperating with different electrolytes, and the structural evolution of MXenes during charge storage. These issues deserve thorough investigations, probably with the assistance of in situ or ex situ characterization techniques, including FTIR, Raman, XRD, XPS, Mössbauer spectroscopy, SEM, and transmission electron microscopy.

ADVANCED
SCIENCE NEWS

www.advancedsciencenews.com

small
methods

www.small-methods.com

Table 1. Summary of the performance of supercapacitors based on $Ti_3C_2T_x$ MXenes.

MXene	Etching method	Morphology	Electrolyte	Electrochemical Performance	Retention	Ref.	Year
$Ti_3C_2T_x$	HCl+LiF	Nanosheets	1 M H_2SO_4	900 F cm^{-3} @ 2 mV s^{-1}	100% (10 000 cycles) @ 10 A g^{-1}	ref. [25]	2014
$Ti_3C_2T_x$	HF	Accordion-like	1 M H_2SO_4	415 F cm^{-3} @ 2 mV s^{-1}	≈100% (10 000 cycles) @ 5 A g^{-1}	ref. [95]	2014
$Ti_3C_2T_x$	CuCl+APS	Accordion-like	1 M $LiPF_6$	738 C g^{-1} @ 0.5 mV s^{-1}	90% (400 cycles) @ 0.5 mV s^{-1}	ref. [100]	2020
$Ti_3C_2T_x$	$CuCl_2$+NaCl+ KCl+TBAOH	Parallel restacked layered	1 M $LiPF_6$ in EC/DC(1:1)	225 mAh g^{-1} @ 0.2 A g^{-1}	72% (2000 cycles) @ 4 A g^{-1}	ref. [102]	2022
$Ti_3C_2T_x$	Microwave- assisted etching	Multilayer hexagonal	3 M KCl	396.17 F g^{-1} @ 1 A g^{-1}	98% (10 000 cycles) @ 1 A g^{-1}	ref. [134]	2023
$Ti_3C_2T_x$	NH_4Cl+TMOAH	Bilayer flake	PVA/H_2SO_4	439 F cm^{-3} @ 10 mV s^{-1}	94.2% (10 000 cycles) @ 5 mA cm^{-2}	ref. [135]	2018
$Ti_3C_2T_x$	HCl+LiF	Nanosheets	LiTFSI–PC	195 F g^{-1} @ 2 mV s^{-1}	94% (10 000 cycles) @ 100 mV s^{-1}	ref. [117]	2019
$Ti_3C_2T_x$	HCl+LiF	Nanosheets	MSA/PVA	1719 mF cm^{-2} @ 100 mA cm^{-2}	92% (80 000 cycles) @ 100 mA cm^{-2}	ref. [136]	2023
$Ti_3C_2T_x$	HCl+LiF	Nanosheets	$EMIMBF_4$	277 µF cm^{-3} @ 1 V s^{-1}	84.6% (4000 cycles) @ 500 V s^{-1}	ref. [137]	2022
$Ti_3C_2T_x$	HCl+LiF	2D layered	EMITFSI	70 F g^{-1} @ 20 mV s^{-1}	80% (1000 cycles) @ 500 mV s^{-1}	ref. [80]	2016
$Ti_3C_2T_x$	HCl+LiF	2D layered	$EMIMBF_4$/PVDF-HFP	96 F cm^{-3} @ 50 mV s^{-1}	92% (1000 cycles) @ 1.5 mA cm^{-2}	ref. [128]	2019
$Ti_3C_2T_x$	HCl+LiF	2D layered	Water-in-LiCl salt gel	19.9 mF cm^{-3} @ 5 mV s^{-1}	≈100% (10 000 cycles) @ 0.1 mA cm^{-2}	ref. [138]	2022
$Ti_3C_2T_x$	HCl+LiF	Macropore structure	3 M H_2SO_4	310 F cm^{-3} @ 10 mV s^{-1}	90% (10 000 cycles) @ 10 A g^{-1}	ref. [62]	2017
$Ti_3C_2T_x$	HCl+LiF	Wavy shape	3 M H_2SO_4	1277 F cm^{-3} @ 10 mV s^{-1}	98.8% (1000 cycles) @100 mV s^{-1}	ref. [119]	2020
$Ti_3C_2T_x$	HCl+HF	Wavy shape	19.8 M LiCl	104 F g^{-1} @ 2 mV s^{-1}	94% (10 000 cycles) @ 1000 mV s^{-1}	ref. [81]	2021
$Ti_3C_2T_x$	HF	3D porous	1 M NaCl	410 F cm^{-3} @ 5 mV s^{-1}	≈100% (5000 cycles) @ 100 mV s^{-1}	ref. [82]	2018
$Ti_3C_2T_x$	HCl+LiF	Continuous micro porous	3 M H_2SO_4	828 F cm^{-3} @ 20 A g^{-1}	90.5% (10 000 cycles) @5 A g^{-1}	ref. [139]	2018
$Ti_3C_2T_x$ aerogel	HCl+LiF	2D layered	3 M H2SO4	414 F g^{-1} @ 1 mV s^{-1}	97% (8000 cycles) @ 4 A g^{-1}	ref. [140]	2019
$Ti_3C_2T_x$-NiO	HCl+LiF	3D porous	1 M Na_2SO_4	341 F cm^{-3} @ 2 mV s^{-1}	99% (1000 cycles) @1 A g^{-1}	ref. [141]	2019
$Ti_3C_2T_x$/SCNT	HCl+LiF	Orderly stacked layers	1 M KOH	220 mF cm^{-3} @ 2 mV s^{-1}	95% (10 000 cycles) @ 5 A g^{-1}	ref. [74]	2018
$Ti_3C_2T_x$/CNTs	HCl+LiF	Orderly stacked layers	1 M Na_2SO_4	1.94 F cm^{-2} @ 3 mA cm^{-2}	94.3% (1000 cycles) @ 50 mV s^{-1}	ref. [75]	2021
$Ti_3C_2T_x$/CNTs	HCl+LiF	Orderly stacked layers	1 M EMITFSI in ACN	245 mF cm^{-3} @ 2 mV s^{-1}	90% (1000 cycles) @ 1 A g^{-1}	ref. [91]	2016
$Ti_3C_2T_x$/PPy	HCl+LiF	2D layered	[EMIM]NTf$_2$	51.85 F g^{-1} @ 20 mV s^{-1}	91% (2000 cycles) @ 0.4 A g^{-1}	ref. [76]	2022
$Ti_3C_2T_x$/rGO	HCl+LiF	Porous	PVA/H_2SO_4	276 F g^{-1} @ 0.5 A g^{-1}	91.3% (10 000 cycles) @ 50 mV s^{-1}	ref. [77]	2022
$Ti_3C_2T_x$/V_2O_5	HF	Lamellar	1 M K_2SO_4	1024 F g^{-1} @ 10 m V^{-1}	96.12% (1000 cycles) @ 60 mV s^{-1}	ref. [142]	2022
$Ti_3C_2T_x$/MnO_2	HCl+LiF	Layered	1 M Na_2SO_4	452 F g^{-1} @ 1 A g^{-1}	80% (2000 cycles) @ 5 A g^{-1}	ref. [143]	2021

(Continued)

2201724 (17 of 21)

**ADVANCED
SCIENCE NEWS**

www.advancedsciencenews.com

**small
methods**

www.small-methods.com

Table 1. (Continued).

MXene	Etching method	Morphology	Electrolyte	Electrochemical Performance	Retention	Ref.	Year
$Ti_3C_2T_x$@CTAB	HF	Pillared	1 M $LiPF_6$ in EC/DEC/EMC (1:1:1)+1 wt%FEC	506 mAh g^{-1} @ 1 A g^{-1}	96.6% (250 cycles) @ 1 A g^{-1}	ref. [84]	2017
$Ti_3C_2T_x$/ $C_{12}E_6$/SWCNTs	LiF+HCl	Vertically aligned	3 M H_2SO_4	200 F g^{-1} @ 2000 mV s^{-1}	≈100% (20 000 cycles) @ 20 A g^{-1}	ref. [81]	2018
$Ti_3C_2T_x$/PANI	LiF+HCl	3D porous	3 M H_2SO_4	1632 F cm^{-3} @ 10 mV s^{-1}	85.7% (20 000 cycles) @ 100 mV s^{-1}	ref. [85]	2020
$Ti_3C_2T_x$/ AC/TEAPW12	LiF+HCl	3D porous	1 M TEABF4 in ACN	76 F g^{-1} @ 1 mV s^{-1}	≈100% (10 000 cycles) @ 2 A g^{-1}	ref. [79]	2022

7) To achieve commercial application of $Ti_3C_2T_x$ MXene electrodes in supercapacitors, the loading density, structural stability, and self-discharging should be further researched and optimized.

Conflict of Interest

The authors declare no conflict of interest.

[1] M. S. Islam, C. A. J. Fisher, *Chem. Soc. Rev.* **2014**, *43*, 185.
[2] N.-S. Choi, Z. Chen, S. A. Freunberger, X. Ji, Y.-K. Sun, K. Amine, G. Yushin, L. F. Nazar, J. Cho, P. G. Bruce, *Angew. Chem., Int. Ed.* **2012**, *51*, 9994.
[3] G. Z. Chen, *Int. Mater. Rev.* **2017**, *62*, 173.
[4] B. E. Conway, *J. Electrochem. Soc.* **1991**, *138*, 1539.
[5] P. Simon, Y. Gogotsi, *Nat. Mater.* **2008**, *7*, 845.
[6] M. Winter, R. J. Brodd, *Chem. Rev.* **2004**, *104*, 4245.
[7] Y. Wang, Y. Song, Y. Xia, *Chem. Soc. Rev.* **2016**, *45*, 5925 .
[8] L. L. Zhang, X. S. Zhao, *Chem. Soc. Rev.* **2009**, *38*, 2520 .
[9] Y. Zhai, Y. Dou, D. Zhao, P. F. Fulvio, R. T. Mayes, S. Dai, *Adv. Mater.* **2011**, *23*, 4828.
[10] E. Raymundo-Piñero, F. Leroux, F. Béguin, *Adv. Mater.* **2006**, *18*, 1877.
[11] M. Kaempgen, C. K. Chan, J. Ma, Y. Cui, G. Gruner, *Nano Lett.* **2009**, *9*, 1872.
[12] J. Gamby, P. L. Taberna, P. Simon, J. F. Fauvarque, M. Chesneau, *J. Power Sources* **2001**, *101*, 109.
[13] R. Kötz, M. Carlen, *Electrochim. Acta* **2000**, *45*, 2483.
[14] W. Wei, X. Cui, W. Chen, D. G. Ivey, *Chem. Soc. Rev.* **2011**, *40*, 1697.
[15] M. Chhowalla, H. S. Shin, G. Eda, L.-J. Li, K. P. Loh, H. Zhang, *Nat. Chem.* **2013**, *5*, 263.
[16] M. Naguib, M. Kurtoglu, V. Presser, J. Lu, J. Niu, M. Heon, L. Hultman, Y. Gogotsi, M. W. Barsoum, *Adv. Mater.* **2011**, *23*, 4248.
[17] M. Naguib, V. N. Mochalin, M. W. Barsoum, Y. Gogotsi, *Adv. Mater.* **2014**, *26*, 992.
[18] P. Urbankowski, B. Anasori, T. Makaryan, D. Er, S. Kota, P. L. Walsh, M. Zhao, V. B. Shenoy, M. W. Barsoum, Y. Gogotsi, *Nanoscale* **2016**, *8*, 11385 .
[19] K. R. G. Lim, M. Shekhirev, B. C. Wyatt, B. Anasori, Y. Gogotsi, Z. W. Seh, *Nat. Synth.* **2022**, *1*, 601.
[20] J. Orangi, M. Beidaghi, *Adv. Funct. Mater.* **2020**, *30*, 2005305.
[21] K. Kannan, K. K. Sadasivuni, A. M. Abdullah, B. Kumar, *Catalysts* **2020**, *10*, 495.
[22] Y. Ma, Y. Yue, H. Zhang, F. Cheng, W. Zhao, J. Rao, S. Luo, J. Wang, X. Jiang, Z. Liu, N. Liu, Y. Gao, *ACS Nano* **2018**, *12*, 3209 .
[23] S. Zhao, H. B. Zhang, J. Q. Luo, Q. W. Wang, B. Xu, S. Hong, Z. Z. Yu, *ACS Nano* **2018**, *12*, 11193 .
[24] M. Hu, Z. Li, H. Zhang, T. Hu, C. Zhang, Z. Wu, X. Wang, *Chem. Commun.* **2015**, *51*, 13531.
[25] M. Ghidiu, M. R. Lukatskaya, M. Q. Zhao, Y. Gogotsi, M. W. Barsoum, *Nature* **2014**, *516*, 78 .
[26] M. M. Hasan, M. M. Hossain, H. K. Chowdhury, *J. Mater. Chem. A* **2021**, *9*, 3231.
[27] G. H. Jeong, S. P. Sasikala, T. Yun, G. Y. Lee, W. J. Lee, S. O. Kim, *Adv. Mater.* **2020**, *32*, 1907006.
[28] B. Raj, A. K. Padhy, S. Basu, M. Mohapatra, *J. Electrochem. Soc.* **2020**, *167*, 136501.
[29] P. Srimuk, F. Kaasik, B. Krüner, A. Tolosa, S. Fleischmann, N. Jäckel, M. C. Tekeli, M. Aslan, M. E. Suss, V. Presser, *J. Mater. Chem. A* **2016**, *4*, 18265.
[30] Z. Wang, Z. Xu, H. Huang, X. Chu, Y. Xie, D. Xiong, C. Yan, H. Zhao, H. Zhang, W. Yang, *ACS Nano* **2020**, *14*, 4916.
[31] J. Luo, E. Matios, H. Wang, X. Tao, W. Li, *InfoMat* **2020**, *2*, 1057.
[32] H. Huang, J. Cui, G. Liu, R. Bi, L. Zhang, *ACS Nano* **2019**, *13*, 3448 .
[33] J. Come, M. Naguib, P. Rozier, M. W. Barsoum, Y. Gogotsi, P. L. Taberna, M. Morcrette, P. Simon, *J. Electrochem. Soc.* **2012**, *159*, A1368.
[34] F. Kong, X. He, Q. Liu, X. Qi, Y. Zheng, R. Wang, Y. Bai, *Ceram. Int.* **2018**, *44*, 11591.
[35] M. Naguib, J. Come, B. Dyatkin, V. Presser, P.-L. Taberna, P. Simon, M. W. Barsoum, Y. Gogotsi, *Electrochem. Commun.* **2012**, *16*, 61.
[36] J. Wu, Y. Wang, Y. Zhang, H. Meng, Y. Xu, Y. Han, Z. Wang, Y. Dong, X. Zhang, *J. Energy Chem.* **2020**, *47*, 203.
[37] M.-S. Cao, Y.-Z. Cai, P. He, J.-C. Shu, W.-Q. Cao, J. Yuan, *Chem. Eng. J.* **2019**, *359*, 1265.
[38] H. Wang, Y. Wu, X. Yuan, G. Zeng, J. Zhou, X. Wang, J. W. Chew, *Adv. Mater.* **2018**, *30*, 1704561.

**ADVANCED
SCIENCE NEWS**

www.advancedsciencenews.com

**small
methods**

www.small-methods.com

[39] A. Feng, Y. Yu, L. Mi, Y. Yu, L. Song, *Ionics* **2019**, *25*, 727.

[40] G. Murali, J. Rawal, J. K. R. Modigunta, Y. H. Park, J.-H. Lee, S.-Y. Lee, S.-J. Park, I. In, *Sustainable Energy Fuels* **2021**, *5*, 5672.

[41] Y. Sun, X. Meng, Y. Dall'Agnese, C. Dall'Agnese, S. Duan, Y. Gao, G. Chen, X.-F. Wang, *Nano-Micro Lett.* **2019**, *11*, 79.

[42] M. Naguib, J. Halim, J. Lu, K. M. Cook, L. Hultman, Y. Gogotsi, M. W. Barsoum, *J. Am. Chem. Soc.* **2013**, *135*, 15966.

[43] M. Naguib, O. Mashtalir, J. Carle, V. Presser, J. Lu, L. Hultman, Y. Gogotsi, M. W. Barsoum, *ACS Nano* **2012**, *6*, 1322.

[44] Z.-W. Gao, W. Zheng, L. Y. S. Lee, *Small* **2019**, *15*, 1902649.

[45] X. Mu, D. Wang, F. Du, G. Chen, C. Wang, Y. Wei, Y. Gogotsi, Y. Gao, Y. Dall'Agnese, *Adv. Funct. Mater.* **2019**, *29*, 1902953.

[46] K. Li, M. Liang, H. Wang, X. Wang, Y. Huang, J. Coelho, S. Pinilla, Y. Zhang, F. Qi, V. Nicolosi, Y. Xu, *Adv. Funct. Mater.* **2020**, *30*, 2000842.

[47] F. Song, G. Li, Y. Zhu, Z. Wu, X. Xie, N. Zhang, *J. Mater. Chem. A* **2020**, *8*, 18538.

[48] N. R. Hemanth, T. Kim, B. Kim, A. H. Jadhav, K. Lee, N. K. Chaudhari, *Mater. Chem. Front.* **2021**, *5*, 3298.

[49] J. Zhou, J. Yu, L. Shi, Z. Wang, H. Liu, B. Yang, C. Li, C. Zhu, J. Xu, *Small* **2018**, *14*, 1803786.

[50] Y. Liu, J. Yu, D. Guo, Z. Li, Y. Su, *J. Alloys Compd.* **2020**, *815*, 152403.

[51] Z. Fan, Y. Wang, Z. Xie, D. Wang, Y. Yuan, H. Kang, B. Su, Z. Cheng, Y. Liu, *Adv. Sci.* **2018**, *5*, 1800750.

[52] Z. Wang, S. Qin, S. Seyedin, J. Zhang, J. Wang, A. Levitt, N. Li, C. Haines, R. Ovalle-Robles, W. Lei, Y. Gogotsi, R. H. Baughman, J. M. Razal, *Small* **2018**, *14*, 1802225.

[53] J. Yan, Y. Ma, C. Zhang, X. Li, W. Liu, X. Yao, S. Yao, S. Luo, *RSC Adv.* **2018**, *8*, 39742 .

[54] M. Boota, Y. Gogotsi, *Adv. Energy Mater.* **2019**, *9*, 1802917.

[55] J. Jimmy, B. Kandasubramanian, *Eur. Polym. J.* **2020**, *122*, 109367.

[56] G. S. Gund, J. H. Park, R. Harpalsinh, M. Kota, J. H. Shin, T.-I. Kim, Y. Gogotsi, H. S. Park, *Joule* **2019**, *3*, 164.

[57] C. Chen, M. Boota, P. Urbankowski, B. Anasori, L. Miao, J. Jiang, Y. Gogotsi, *J. Mater. Chem. A* **2018**, *6*, 4617.

[58] F. Bu, M. M. Zagho, Y. Ibrahim, B. Ma, A. Elzatahry, D. Zhao, *Nano Today* **2020**, *30*, 100803.

[59] J. Li, X. Yuan, C. Lin, Y. Yang, L. Xu, X. Du, J. Xie, J. Lin, J. Sun, *Adv. Energy Mater.* **2017**, *7*, 1602725.

[60] C. Zhang, B. Anasori, A. Seral-Ascaso, S.-H. Park, N. McEvoy, A. Shmeliov, G. S. Duesberg, J. N. Coleman, Y. Gogotsi, V. Nicolosi, *Adv. Mater.* **2017**, *29*, 1702678.

[61] C. Yang, Y. Tang, Y. Tian, Y. Luo, M. Faraz Ud Din, X. Yin, W. Que, *Adv. Energy Mater.* **2018**, *8*, 1802087.

[62] M. R. Lukatskaya, S. Kota, Z. Lin, M.-Q. Zhao, N. Shpigel, M. D. Levi, J. Halim, P.-L. Taberna, M. W. Barsoum, P. Simon, Y. Gogotsi, *Nat. Energy* **2017**, *2*, 17105.

[63] M. Yao, Y. Chen, Z. Wang, C. Shao, J. Dong, Q. Zhang, L. Zhang, X. Zhao, *Chem. Eng. J.* **2020**, *395*, 124057.

[64] M. R. Lukatskaya, S.-M. Bak, X. Yu, X.-Q. Yang, M. W. Barsoum, Y. Gogotsi, *Adv. Energy Mater.* **2015**, *5*, 1500589.

[65] M. Okubo, A. Sugahara, S. Kajiyama, A. Yamada, *Acc. Chem. Res.* **2018**, *51*, 591.

[66] Y. Gao, L. Wang, Z. Li, Y. Zhang, B. Xing, C. Zhang, A. Zhou, *J. Adv. Ceram.* **2015**, *4*, 130.

[67] Q. X. Xia, N. M. Shinde, T. Zhang, J. M. Yun, A. Zhou, R. S. Mane, S. Mathur, K. H. Kim, *Dalton Trans.* **2018**, *47*, 8676.

[68] L. Yu, L. Hu, B. Anasori, Y.-T. Liu, Q. Zhu, P. Zhang, Y. Gogotsi, B. Xu, *ACS Energy Lett.* **2018**, *3*, 1597.

[69] G. Li, L. Tan, Y. Zhang, B. Wu, L. Li, *Langmuir* **2017**, *33*, 9000.

[70] F. Han, S. Luo, L. Xie, J. Zhu, W. Wei, X. Chen, F. Liu, W. Chen, J. Zhao, L. Dong, K. Yu, X. Zeng, F. Rao, L. Wang, Y. Huang, *ACS Appl. Mater. Interfaces* **2019**, *11*, 8443.

[71] M. R. Lukatskaya, O. Mashtalir, C. E. Ren, Y. Dall'Agnese, P. Rozier, P. L. Taberna, M. Naguib, P. Simon, M. W. Barsoum, Y. Gogotsi, *Science* **2013**, *341*, 1502.

[72] H. Shao, Z. Lin, K. Xu, P.-L. Taberna, P. Simon, *Energy Storage Mater.* **2019**, *18*, 456.

[73] a) B. Aubrey, My Contributions (Photo Gallery): Summit Lake, Akshayuk Pass, Baffin Is https://en.wikipedia.org/wiki/User: BrettA343 (accessed: April 2023); b) J. Misachi, What Is A Cliff And How Is It Formed? https://www.worldatlas.com/articles/what-is-a-cliff-and-how-is-it-formed.html. (accessed: April 2023)

[74] Q. Fu, X. Wang, N. Zhang, J. Wen, L. Li, H. Gao, X. Zhang, *J. Colloid Interface Sci.* **2018**, *511*, 128.

[75] X. Li, J. Zhu, W. Liang, I. Zhitomirsky, *Mater. Chem. Phys.* **2021**, *268*, 124748.

[76] Q. Fan, R. Zhao, M. Yi, P. Qi, C. Chai, H. Ying, J. Hao, *Chem. Eng. J.* **2022**, *428*, 131107.

[77] J. Zhang, D. Jiang, L. Liao, L. Cui, R. Zheng, J. Liu, *Chem. Eng. J.* **2022**, *429*, 132232.

[78] G. Z. Chen, *Prog. Nat. Sci.: Mater. Int.* **2021**, *31*, 792.

[79] J.-J. Zhu, A. Hemesh, J. J. Biendicho, L. Martinez-Soria, D. Rueda-Garcia, J. R. Morante, B. Ballesteros, P. Gomez-Romero, *J. Colloid Interface Sci.* **2022**, *623*, 947.

[80] Z. Lin, D. Barbara, P.-L. Taberna, L. Van Aken K, B. Anasori, Y. Gogotsi, P. Simon, *J. Power Sources* **2016**, *326*, 575.

[81] Y. Xia, T. S. Mathis, M. Q. Zhao, B. Anasori, A. Dang, Z. Zhou, H. Cho, Y. Gogotsi, S. Yang, *Nature* **2018**, *557*, 409.

[82] W. Bao, X. Tang, X. Guo, S. Choi, C. Wang, Y. Gogotsi, G. Wang, *Joule* **2018**, *2*, 778.

[83] J. Luo, C. Wang, H. Wang, X. Hu, E. Matios, X. Lu, W. Zhang, X. Tao, W. Li, *Adv. Funct. Mater.* **2019**, *29*, 1805946.

[84] J. Luo, W. Zhang, H. Yuan, C. Jin, L. Zhang, H. Huang, C. Liang, Y. Xia, J. Zhang, Y. Gan, X. Tao, *ACS Nano* **2017**, *11*, 2459 .

[85] K. Li, X. Wang, S. Li, P. Urbankowski, J. Li, Y. Xu, Y. Gogotsi, *Small* **2020**, *16*, 1906851.

[86] L. Yu, Z. Fan, Y. Shao, Z. Tian, J. Sun, Z. Liu, *Adv. Energy Mater.* **2019**, *9*, 1901839.

[87] T.-H. Chang, T. Zhang, H. Yang, K. Li, Y. Tian, J. Y. Lee, P.-Y. Chen, *ACS Nano* **2018**, *12*, 8048.

[88] A. Qian, S. E. Hyeon, J. Y. Seo, C.-H. Chung, *Electrochim. Acta* **2018**, *266*, 86.

[89] C. Zhan, M. Naguib, M. Lukatskaya, P. R. C. Kent, Y. Gogotsi, J. D-e, *J. Phys. Chem. Lett.* **2018**, *9*, 1223.

[90] M. M. Baig, I. H. Gul, S. M. Baig, F. Shahzad, *J. Electroanal. Chem.* **2022**, *904*, 115920.

[91] Y. Dall'Agnese, P. Rozier, P.-L. Taberna, Y. Gogotsi, P. Simon, *J. Power Sources* **2016**, *306*, 510.

[92] K. Liang, R. A. Matsumoto, W. Zhao, N. C. Osti, I. Popov, B. P. Thapaliya, S. Fleischmann, S. Misra, K. Prenger, M. Tyagi, E. Mamontov, V. Augustyn, R. R. Unocic, A. P. Sokolov, S. Dai, P. T. Cummings, M. Naguib, *Adv. Funct. Mater.* **2021**, *31*, 2104007.

[93] X. Wang, T. S. Mathis, Y. Sun, W.-Y. Tsai, N. Shpigel, H. Shao, D. Zhang, K. Hantanasirisakul, F. Malchik, N. Balke, J. D-e, P. Simon, Y. Gogotsi, *ACS Nano* **2021**, *15*, 15274 .

[94] M. Cao, F. Wang, L. Wang, W. Wu, W. Lv, J. Zhu, *J. Electrochem. Soc.* **2017**, *164*, A3933.

[95] Y. Dall'Agnese, M. R. Lukatskaya, K. M. Cook, P.-L. Taberna, Y. Gogotsi, P. Simon, *Electrochem. Commun.* **2014**, *48*, 118.

[96] Y. Tang, J. Zhu, C. Yang, F. Wang, *J. Electrochem. Soc.* **2016**, *163*, A1975.

[97] X. Zhang, Y. Liu, S. Dong, J. Yang, X. Liu, *Electrochim. Acta* **2019**, *294*, 233.

[98] R. B. Rakhi, B. Ahmed, M. N. Hedhili, D. H. Anjum, H. N. Alshareef, *Chem. Mater.* **2015**, *27*, 5314.

[99] F. Yan, C. Zhang, H. Wang, X. Zhang, H. Zhang, H. Jia, Y. Zhao, J. Wang, *J. Mater. Chem. A* **2021**, *9*, 442.

[100] Y. Li, H. Shao, Z. Lin, J. Lu, L. Liu, B. Duployer, P. O. A. Persson, P. Eklund, L. Hultman, M. Li, K. Chen, X. H. Zha, S. Du, P. Rozier, Z. Chai, E. Raymundo-Pinero, P. L. Taberna, P. Simon, Q. Huang, *Nat. Mater.* **2020**, *19*, 894 .

[101] K. Arole, J. W. Blivin, S. Saha, D. E. Holta, X. Zhao, A. Sarmah, H. Cao, M. Radovic, J. L. Lutkenhaus, M. J. Green, *iScience* **2021**, *24*, 103403.

[102] L. Liu, M. Orbay, S. Luo, S. Duluard, H. Shao, J. Harmel, P. Rozier, P. L. Taberna, P. Simon, *ACS Nano* **2022**, *16*, 111.

[103] X. Li, Z. Huang, C. Zhi, *Front. Mater.* **2019**, *6*, 312.

[104] H. Dong, P. Xiao, N. Jin, B. Wang, Y. Liu, Z. Lin, *ChemElectroChem* **2021**, *8*, 957.

[105] M. Li, J. Lu, K. Luo, Y. Li, K. Chang, K. Chen, J. Zhou, J. Rosen, L. Hultman, P. Eklund, P. O. Å. Persson, S. Du, Z. Chai, Z. Huang, Q. Huang, *J. Am. Chem. Soc.* **2019**, *141*, 4730 .

[106] J. Tang, T. S. Mathis, N. Kurra, A. Sarycheva, X. Xiao, M. N. Hedhili, Q. Jiang, H. N. Alshareef, B. Xu, F. Pan, Y. Gogotsi, *Angew. Chem., Int. Ed. Engl.* **2019**, *58*, 17849.

[107] X. Chen, Y. Zhu, M. Zhang, J. Sui, W. Peng, Y. Li, G. Zhang, F. Zhang, X. Fan, *ACS Nano* **2019**, *13*, 9449.

[108] A. Iqbal, J. Hong, T. Y. Ko, C. M. Koo, *Nano Convergence* **2021**, *8*, 9.

[109] M. G. Jung, G. Sambhaji Gund, Y. Gogotsi, H. S. Park, *Batteries Supercaps* **2020**, *3*, 354.

[110] Y. Liu, Y. Jiang, Z. Hu, J. Peng, W. Lai, D. Wu, S. Zuo, J. Zhang, B. Chen, Z. Dai, Y. Yang, Y. Huang, W. Zhang, W. Zhao, W. Zhang, L. Wang, S. Chou, *Adv. Funct. Mater.* **2021**, *31*, 2008033.

[111] Z. Xiao, C. Lei, C. Yu, X. Chen, Z. Zhu, H. Jiang, F. Wei, *Energy Storage Mater.* **2020**, *24*, 565.

[112] C. Choi, D. S. Ashby, D. M. Butts, R. H. DeBlock, Q. Wei, J. Lau, B. Dunn, *Nat. Rev. Mater.* **2020**, *5*, 5.

[113] S. Fleischmann, J. B. Mitchell, R. Wang, C. Zhan, D. E. Jiang, V. Presser, V. Augustyn, *Chem. Rev.* **2020**, *120*, 6738.

[114] T. C. Liu, W. G. Pell, B. E. Conway, S. L. Roberson, *J. Electrochem. Soc.* **1998**, *145*, 1882.

[115] J. Peng, Y. Deng, D. Wang, X. Jin, G. Z. Chen, *J. Electroanal. Chem.* **2009**, *627*, 28.

[116] J. Wang, J. Polleux, J. Lim, B. Dunn, *J. Phys. Chem. C* **2007**, *111*, 14925.

[117] X. Wang, T. S. Mathis, K. Li, Z. Lin, L. Vlcek, T. Torita, N. C. Osti, C. Hatter, P. Urbankowski, A. Sarycheva, M. Tyagi, E. Mamontov, P. Simon, Y. Gogotsi, *Nat. Energy* **2019**, *4*, 241.

[118] V. Augustyn, P. Simon, B. Dunn, *Energy Environ. Sci.* **2014**, *7*, 1597.

[119] Q. Jiang, N. Kurra, M. Alhabeb, Y. Gogotsi, H. N. Alshareef, *Adv. Energy Mater.* **2018**, *8*, 1703043.

[120] Q. Wu, Y. Wang, P. Li, S. Chen, F. Wu, *Appl. Phys. A* **2021**, *127*, 822.

[121] S. Cho, D. Y. Kim, Y. Seo, *Adv. Mater. Interfaces* **2020**, *7*, 2000750.

[122] J. H. Chae, G. Z. Chen, *Electrochim. Acta* **2012**, *86*, 248.

[123] L. Demarconnay, E. Raymundo-Piñero, F. Béguin, *J. Power Sources* **2011**, *196*, 580.

[124] J. Huang, Z. Guo, Y. Ma, D. Bin, Y. Wang, Y. Xia, *Small Methods* **2019**, *3*, 1800272.

[125] C. Y. Foo, A. Sumboja, D. J. H. Tan, J. Wang, P. S. Lee, *Adv. Energy Mater.* **2014**, *4*, 1400236.

[126] M. Sun, G. Wang, C. Yang, H. Jiang, C. Li, *J. Mater. Chem. A* **2015**, *3*, 3880.

[127] H. Avireddy, B. W. Byles, D. Pinto, J. M. Delgado Galindo, J. J. Biendicho, X. Wang, C. Flox, O. Crosnier, T. Brousse, E. Pomerantseva, J. R. Morante, Y. Gogotsi, *Nano Energy* **2019**, *64*, 103961.

[128] S. Zheng, C. Zhang, F. Zhou, Y. Dong, X. Shi, V. Nicolosi, Z.-S. Wu, X. Bao, *J. Mater. Chem. A* **2019**, *7*, 9478.

[129] N. C. Osti, M. W. Thompson, L. Van Aken K, M. Alhabeb, M. Tyagi, J.-K. Keum, P. T. Cummings, Y. Gogotsi, E. Mamontov, *J. Phys. Chem. C* **2018**, *122*, 27561.

[130] A. J. Bard, L. R. Faulkner, H. S. White, *Electrochemical Methods: Fundamentals and Applications*, John Wiley & Sons, New York **2022**.

[131] N. Jäckel, B. Krüner, K. L. Van Aken, M. Alhabeb, B. Anasori, F. Kaasik, Y. Gogotsi, V. Presser, *ACS Appl. Mater. Interfaces* **2016**, *8*, 32089.

[132] Z. Lin, P. Rozier, B. Duployer, P.-L. Taberna, B. Anasori, Y. Gogotsi, P. Simon, *Electrochem. Commun.* **2016**, *72*, 50.

[133] K. Kim, Y. Ando, A. Sugahara, S. Ko, Y. Yamada, M. Otani, M. Okubo, A. Yamada, *Chem. Mater.* **2019**, *31*, 5190.

[134] Q. Wu, Y. Xue, P. Li, Y. Wang, F. Wu, *Appl. Surf. Sci.* **2023**, *609*, 155329.

[135] S. Yang, P. Zhang, F. Wang, A. G. Ricciardulli, M. R. Lohe, P. W. M. Blom, X. Feng, *Angew. Chem., Int. Ed.* **2018**, *57*, 15491.

[136] C. Liu, H. Wu, X. Wang, J. Fan, H. Su, D. Yang, Y. Wei, F. Du, Y. Dall'Agnese, Y. Gao, *Energy Storage Mater.* **2023**, *54*, 164.

[137] X. Feng, S. Wang, P. Das, X. Shi, S. Zheng, F. Zhou, J. Ning, D. Wang, J. Zhang, Y. Hao, Z.-S. Wu, *J. Energy Chem.* **2022**, *69*, 1.

[138] Y. Zhu, S. Zheng, P. Lu, J. Ma, P. Das, F. Su, H.-M. Cheng, Z.-S. Wu, *Natl. Sci. Rev.* **2022**, *9*, nwac024.

[139] Z. Fan, Y. Wang, Z. Xie, X. Xu, Y. Yuan, Z. Cheng, Y. Liu, *Nanoscale* **2018**, *10*, 9642.

[140] X. Zhang, X. Liu, S. Dong, J. Yang, Y. Liu, *Appl. Mater. Today* **2019**, *16*, 315.

[141] T. Shang, Z. Lin, C. Qi, X. Liu, P. Li, Y. Tao, Z. Wu, D. Li, P. Simon, Q.-H. Yang, *Adv. Funct. Mater.* **2019**, *29*, 1903960.

[142] T. Tahir, D. Alhashmialameer, S. Zulfiqar, A. M. E. Atia, M. F. Warsi, K. Chaudhary, H. M. El Refay, *Ceram. Int.* **2022**, *48*, 24840.

[143] X. Zhang, B. Shao, A. Guo, Z. Sun, J. Zhao, F. Cui, X. Yang, *Appl. Surf. Sci.* **2021**, *560*, 150040.

Tingting Jiang received her B.Sc. in materials science and engineering from Zhejiang University in 2009, and Ph.D. in materials physics and chemistry from Zhejiang University and State Key lab of Silicon Materials in 2014. Currently, she is an associate professor at Wuhan University of Science and Technology. Her research interests are designs and mechanisms of electrochemical energy storage materials such as high-capacity lithium-ion battery electrode materials.

2201724 (20 of 21)

**ADVANCED
SCIENCE NEWS**

www.advancedsciencenews.com

**small
methods**

www.small-methods.com

Yichen Wang obtained her Bachelor's degree in polymer material and engineering from Hubei University of Technology in 2022. She is now a postgraduate student in materials science and engineering at Wuhan University of Science and Technology. Her main research interest is silicon-based negative electrodes for lithium-ion batteries.
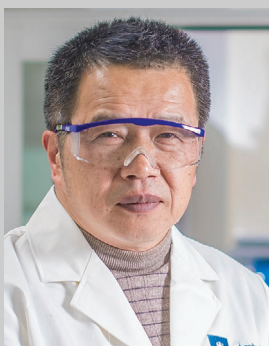
George Z. Chen has graduated from Jiujiang Teachers Training College with a Diploma in 1981, Fujian Normal University with an M.Sc. in 1985, and the University of London/Imperial College with a Ph.D./DIC in 1992. After contracted work at Universities of Oxford, Leeds, Cambridge, and Wuhan, he joined Nottingham University in 2003 as Reader, and became professor in 2009. He was invited professor at the Université de la Mediterranée and Wuhan University of Science and Technology. Supported by government, industry, and families of students, he has led research on electrochemical technologies in association with molten salts and ionic liquids for materials, energy, and environment.